

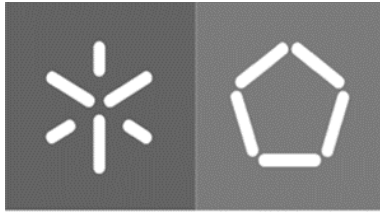


Ana Rita Pacheco Cacho

Microfluidic-based isolation of rare-tumor associated cells in prostate cancer

Universidade do Minho
Escola de Engenharia





Universidade do Minho
Escola de Engenharia

Ana Rita Pacheco Cacho

**Microfluidic-based isolation of rare-tumor
associated cells in prostate cancer**

Dissertação de Mestrado
Mestrado Integrado em Engenharia Biomédica

Trabalho efetuado sob a orientação de
Doutora Sandra Carvalho
Professor Doutor Rui Alberto Lima

abril de 2021

DIREITOS DE AUTOR E CONDIÇÕES DE UTILIZAÇÃO DO TRABALHO POR TERCEIROS

Este é um trabalho académico que pode ser utilizado por terceiros desde que respeitadas as regras e boas práticas internacionalmente aceites, no que concerne aos direitos de autor e direitos conexos.

Assim, o presente trabalho pode ser utilizado nos termos previstos na licença abaixo indicada. Caso o utilizador necessite de permissão para poder fazer um uso do trabalho em condições não previstas no licenciamento indicado, deverá contactar o autor, através do RepositóriUM da Universidade do Minho.



Atribuição-NãoComercial-SemDerivações
CC BY-NC-ND

<https://creativecommons.org/licenses/by-nc-nd/4.0/>

This work results of the project InNPeC - Nano tools for rare giants: an innovative blood-based screening for prostate cancer (POCI-01-0145-FEDER-031442), funded by European Regional Development Found (ERDF) and by Fundação para Ciencia e Tecnologia (FCT).



ACKNOWLEDGEMENTS

Firstly, I would like to thank Sandra Carvalho, *PhD*, from the International Iberian Nanotechnology Laboratory (INL), for introducing and accepting me in this project and in the Nanodevices group. I am very grateful for all the availability, support and guidance, as well as the knowledge she shared in the course of this work. I also thank Diana Pinho, *PhD* for supervising my work and supporting me, not only regarding this project but also concerning my professional future. I want to thank both for constant daily support.

Secondly, I want to acknowledge Professor Rui Lima for all support. I would like to acknowledge Professor Paulo Freitas, Director-general of INL, for all the help and support provided in this project.

This work was only possible with the collaboration of Hospital of Braga and Clinical Academic Center- Braga (2CA). Within this department, I would like to acknowledge Dr. António Marques and Rosana Magalhães, for establishing the project partnership between Hospital and INL.

I would like to acknowledge my friends, who directly or indirectly supported me during this phase, having an important role in the elaboration of this work. I want to thank Luis Tenente for encouraging me in complicated times, for the emotional support endless other things. Last but not least, I would like to thank my family, especially my parents, Manuel Cacho and Maria Emília Cacho, for their support in this academic journey. To my Brother Luis, for the friendship and positive spirit that helped to facilitate and lead me to overcome academic challenges. Everything I have accomplished in life; I owe it to them. This experience would have not been the same without them.

STATEMENT OF INTEGRITY

I hereby declare having conducted this academic work with integrity. I confirm that I have not used plagiarism or any form of undue use of information or falsification of results along the process leading to its elaboration.

I further declare that I have fully acknowledged the Code of Ethical Conduct of the University of Minho.

ABSTRACT

Prostate cancer (PCa) is the most common neoplasia among men. About 90 000 European man die each year from metastatic disease that targets primarily the bones, highlighting the unmet need for new diagnostic tools and therapies. Liquid biopsy has recently been exploited as a promising non-invasive tool towards the molecular profiling of circulating cancer associated cells in various biological fluids, envisaging early diagnosis and real-time patient monitoring of cancer. Among those cells, circulating tumour cells (CTCs), released from the primary tumour into the bloodstream, are considered the main promoters of metastasis. Efficient technologies able to isolate and detect all CTC subpopulations, particularly those most capable of establishing overt metastasis, are urgently required. Other atypical cell population identified in peripheral blood of PCa patients is the cancer-associated macrophages-like cells (CAMLs) that have been reported to interact with CTCs, hitting a role for CAMLs in cancer cell dissemination. Remarkably, CAMLs are more prevalent than CTCs, responsive to treatment and may detect cancer while absent in healthy subjects.

In this study, microfluidic cell capture devices have been designed and fabricated for optimized isolation of both CTCs and CAMLs from peripheral blood of PCa patients. Isolation is based on the particular physical characteristics of both target cell populations that allow independent cell collection, *in situ* molecular characterization and further *in vitro* culturing. For optimization purposes, monocytes-derived giant cells were firstly generated *in vitro*, combined with prostate cancer cell line, and spiked in healthy donor blood to be then run into the microfluidic device at different flow rates. Efficiencies of 87% and 43% were obtained in the isolation of PCa cells and monocytes-derived giant cells, respectively (with the flow rate of 100 $\mu\text{L}/\text{min}$ for the working fluid and 1000 $\mu\text{L}/\text{min}$ for the buffer). Purity of 71% was also achieved. Further experiments with clinical samples from PCa patients are going to be performed in an optimized microfluidic device prototype. The collected two independent cell populations will be then phenotypically characterized in order to find the appropriate combination of molecular markers targeting CTCs and CAMLs and also elucidate about novel molecular targets for future therapeutic approaches.

Key words: Biomedical microdevices, CAMLs, CTCs, Metastasis, Microfluidics, Prostate cancer.

RESUMO

O cancro da próstata é considerado a neoplasia mais comum entre os homens. Cerca de 90.000 homens europeus morrem em cada ano de doenças metastáticas que atingem principalmente os ossos, destacando a necessidade de novas ferramentas e terapias de diagnóstico. A biópsia líquida começou a ser recentemente explorada como uma ferramenta não invasiva promissora para o perfil molecular de células associadas ao cancro em circulação em vários fluidos biológicos, promovendo o diagnóstico precoce e a monitorização em tempo real do paciente. Entre essas células, destacam-se as células tumorais circulantes (CTCs), que são libertadas do tumor primário entrando na corrente sanguínea. Estas células são consideradas os principais promotores de metástases. Por este motivo, são urgentemente necessárias tecnologias eficientes capazes de isolar e detetar todas as subpopulações de CTCs, particularmente as com maior potencial metastático. Outra população de células atípicas identificada no sangue periférico de pacientes com cancro de próstata são as células semelhantes a macrófagos associados a cancro (CAMLs) que têm vindo a ser relatadas por interagirem com as CTCs, desempenhando um papel importante na disseminação de células cancerígenas.

As CAMLs são mais prevalentes que as CTCs, apresentam resposta ao tratamento e apenas podem ser detetadas em pacientes com cancro, sendo assim, ausentes em indivíduos saudáveis.

Neste estudo, dispositivos de microfluídica para a captura de células foram projetados e fabricados para isolamento otimizado de CTCs e CAMLs do sangue periférico de pacientes com cancro de próstata. O isolamento é baseado nas características físicas de ambas as populações de células-alvo que permitem a recolha independente de células, caracterização molecular *in situ* e posterior cultivo *in vitro*. Para fins de otimização, as células gigantes derivadas de monócitos foram geradas *in vitro*, combinadas com a linha celular do cancro de próstata, e adicionadas no sangue de doadores saudáveis para serem introduzidas em microdispositivos com diferentes caudais. Eficiências de 87% e 43% foram obtidas no isolamento de células do cancro da próstata e células gigantes derivadas de monócitos, respetivamente (caudal de 100 $\mu\text{L}/\text{min}$ para o fluido de trabalho e 1000 $\mu\text{L}/\text{min}$ para a solução tampão). Também foi alcançada uma pureza de 71%. Experiências com amostras clínicas de

pacientes com cancro de próstata necessitam de ser realizadas no protótipo final do dispositivo microfluídico. As duas populações celulares serão posteriormente caracterizadas fenotipicamente, a fim de encontrar a combinação apropriada de marcadores moleculares para as CTCs e CAMLs e também elucidar sobre novos alvos moleculares para futuras abordagens terapêuticas.

Palavras-chaves: CAMLs, Cancro da Próstata, CTCs, metastização, microdispositivo biomédico, microfluídica.

CONTENTS

ACKNOWLEDGEMENTS	v
ABSTRACT	vii
RESUMO	ix
CONTENTS	xi
LIST OF FIGURES	xiii
LIST OF TABLES	xvii
NOMENCLATURE	xviii
1. STATE OF ART	1
1.1. Prostate Cancer	1
1.1.1. Epidemiology and Aetiology.....	1
1.1.2. Prostate Carcinogenesis	2
1.1.3. Diagnostic tools for prostate cancer	4
1.1.4. Molecular biomarkers	5
1.1.5. Metastization	7
1.1.6. Liquid Biopsies	8
1.2. Microfluidics in cell biology.....	11
1.2.1. Technical concepts of biofluids	11
1.2.2. Blood Flow and its constituents	13
1.2.3. Microfluidic technologies for cell isolation	13
1.2.4. CTCs and CAMLs isolation: standard methods.....	14
1.2.5. Label-free cell isolation: microfluidic technologies.....	15
1.2.6. Fabrication of microfluidic systems	19
1.3. Aims	23
2. MATERIALS AND METHODS	25
2.1. Cell culture.....	25
2.2. Isolation and culture of monocytes	25
2.3. In vitro generation of giant cells	27

2.4.	Design considerations of microfluidic devices	27
2.5.	Fabrication of the microfluidic devices	30
2.6.	Set up preparation of microfluidic system.....	31
2.7.	Flow rates optimization.....	32
2.8.	Spiking Experiments	32
2.9.	Analysis of cells isolation	33
2.10.	Cell viability	33
2.11.	Statistical Analysis	34
3.	RESULTS AND DISCUSSION	35
3.1.	In vitro generation of giant cells	35
3.2.	Devices characterization and working principle	38
3.3.	Devices flow rates optimization	41
3.4.	DU-145 and Giant cells microfluidic-based efficiency	44
3.5.	Viability of isolated cells from microfluidic devices.....	51
4.	CONCLUSION AND FUTURE WORK.....	53
	REFERENCES	55
	ANNEXES.....	66

LIST OF FIGURES

Figure 1- PCa incidence and mortality rate of the 10 most common cancers for males in Portugal 2018. Adapted from Globocan. 1

Figure 2- Estimated age-standardized incidence and mortality rates (world) in 2018, prostate, males. Adapted from Globocan..... 2

Figure 3- Prostate carcinogenesis. Morphological features of different stages of PCa progression are correlated with the molecular landscape. Prostate epithelial cells are shown in pink, the stromal cells in green and the basement membrane separating the epithelial and stromal cell compartments is shown in blue. 3

Figure 4- The role of CTCs in tumor metastasis. 1) Tumor cells enter the circulation 2) arrest of CTC in the blood stream; 3) CTC adhere to blood vessel walls and extravasate to distant sites; 4) The majority of cell die, while others enter a latent state as single cells or develop into secondary tumors. Adapted from Cho et al., 2018. 7

Figure 5- Variation of Shear stress and viscosity with the shear rate for a Newtonian and Pseudoplastic fluid..... 12

Figure 6- Classification of microfluidics isolation methods. Adapted from Yan et al., 2017.... 16

Figure 7- Photolithography steps with positive and negative photoresist. Adapted from Bellah et al., 2012..... 20

Figure 8- Soft lithography to fabricate microfluidic devices in PDMS. Adapted from Vera et al., 2015..... 21

Figure 9- Manufactures guidelines for the use of RosetteSep™ human monocyte enrichment cocktail kit.1- add Rosette Antibody cocktail; 2- layer the diluted blood over density gradient; 3- centrifuge for 20 min to separate the enriched cells; 4- collect the layer with the monocytes. 25

Figure 10- Monocytes isolation. (A) Layers resulted from first centrifugation in order to remove the plasma (B) layers resulted from density gradient centrifugation of sample. 26

Figure 11- Schematic cross section of a curved microchannel, illustrating the focusing positions of particles of varied size. The lift force and the Dean Drag force are highlighted..... 28

Figure 12- Design in AutoCAD software with the respective lengths of inlets and outlets (A) device with two inlets and two outlets; (B) device with two inlets and four outlets. 29

Figure 13- Silicon wafer with the devices moulds fabricated by photolithography: (A) device with two inlets and two outlets; (B) device with two inlets and four outlets. 30

Figure 14- Schematic representation of the spiking experiments: 50, 100, 1000, and 2000 DU-145 or giant cells pre-stained with DAPI and Calcein-AM were spiked s in the diluted blood and run into the device with two inlets and two outlets with the flow rates of sample/buffer at 100/1000 $\mu\text{L}/\text{min}$, then the recovered outlet 2 was centrifuged, reduced to 1000 μL and run into the device with two inlets and four outlets with the flow rates of sample/buffer at 100/1000 $\mu\text{L}/\text{min}$. The cells obtained in each outlet were counted under fluorescence microscope..... 33

Figure 15- Schematic representation of the viability assays: 1000 DU-145 and Giant cells pre-stained with DAPI were spiked into PBS and run into the device with two inlets and two outlets with the flow rates of sample/buffer at 100/1000 $\mu\text{L}/\text{min}$. Then the recovered outlets (outlet 1 and 2) were centrifuged, reduced to 500 μL , and run into the device with two inlets and four outlets with the flow rates of sample/buffer at 100/1000 $\mu\text{L}/\text{min}$. Once again, all four outlets were recovered together, centrifuged, and run into a third microfluidic platform. Then the cells were counted under fluorescence microscope. 34

*Figure 16- In vitro generation of giant cells. (A) Phase contrast images of giant cells after 10 days of treatment with cytokines. Scale bar 100 μm (B) Mean of area of adhered cells after 10 days of treatment with cytokines. Results are described as Mean +SD. * $p < 0.01$, ** $p < 0.005$ and **** $p < 0.0001$ 36*

*Figure 17- Suspended giant cells in the end of treatment with cytokines (A). Phase contrast images of giant cells after detachment from the plastic culture flask. Scale bar 100 μm (B) mean of area of suspended cells in function to the treatment that was applied. Results are described as Mean +SD of 1 independent experiments. * $p < 0.01$, ** $p < 0.005$ and **** $p < 0.0001$ 37*

Figure 18- Working principle of the microfluidic system: larger target microparticles achieve full focusing on inner wall while non-target particles achieve the full focusing in the external wall (A) device with 2 inlets and 2 outlets. Scale bar 100 μm ; (B) device with 2 inlets and 4 outlets. Scale bar 100 μm 39

Figure 19- Size distribution of DU-45 cells. Key statistical parameters of DU-145 cells (diameter): min 11.008 μm ; max 21.075 μm ; mean 15.1974 μm ; SD: 2.954 μm 41

Figure 20- Size distribution giant cells Key statistical parameters of giant cells (diameter): min 12.172 μm ; max 61.3685 μm ; mean 28.412 μm ; SD: 9.263 μm 42

Figure 21- Average isolation efficiency obtained for each device of giant cells and Du-145 of three different experiments for runs at different flow rates of sample/buffer ratio. (A) Giant cells suspended into PBS and run in the device with 2 inlets/2 outlets; (B) DU-145 suspended into PBS and run in the Device with 2 inlets/2 outlets; (C) Giant cells suspended into PBS and run in the Device with 2 inlets/4 outlets; (D) DU-145 suspended into PBS and run in the Device with 2 inlets/4 outlets. Results are described as Mean +SD of 3 independent experiments. * $p < 0.01$, ** $p < 0.005$ and **** $p < 0.0001$ 43

Figure 22- Cells < 20 μm depletion in function to the number of cells spiked in diluted blood and Cells < 20 μm isolated by the device (A) Schematic identification of the target outlets; (B) Average depletion of cells < 20 μm per outlet of three different experiments. 50, 100, 1000 and 2000 spiked cells in the diluted blood were run into the device with 2 inlets and 2 outlets with the flow rates of sample/buffer at 100/1000 $\mu\text{L}/\text{min}$, then the recovered outlet 2 was centrifuged, reduced to 1000 μL and run into the device with 2 inlets and 4 outlets with the flow rates of sample/buffer at 100/1000 $\mu\text{L}/\text{min}$. Results are described as Mean +SD of 3 independent experiments. (C) Cells <20 μm pre-stained with DAPI recovered. Images obtained with the objective lens of 20x. Scale bar 30 μm . * $p < 0.01$, ** $p < 0.005$ and **** $p < 0.0001$ 45

Figure 23- Cells > 20 μm recovery in function to the number of cells spiked in diluted blood (A) Schematic identification of the isolation microfluidic system and target outlets; (B) Average recovery rate of three different experiments. 50, 100, 1000 and 2000 spiked cells in the diluted blood were run into the device with 2 inlets and 2 outlets with the flow rates of sample/buffer at 100/1000 $\mu\text{L}/\text{min}$, then the recovered outlet 2 was centrifuged, reduced to 1000 μL and run into the device with 2 inlets and 4 outlets with the flow rates of sample/buffer at 100/1000 $\mu\text{L}/\text{min}$. Error bars represent standard deviation; Results are described as Mean +SD of 3 independent experiments (C) Average recovery rate of cells > 20 μm per outlet in function of the isolated cells for three different experiments. 50, 100, 1000 and 2000 spiked cells in the diluted blood were run into the device with 2 inlets and 2 outlets with the flow rates of sample/buffer at 100/1000 $\mu\text{L}/\text{min}$, then the recovered outlet 2 was centrifuged, reduced to 1000 μL , and run into the device with 2 inlets and 4 outlets with the flow rates of sample/buffer at 100/1000 $\mu\text{L}/\text{min}$. Error bars represent standard deviation. Results are described as Mean

+SD of 3 independent experiments (D) Cells >20 μm pre-stained with Calcein-AM recovered. Images obtained with the objective lens of 20x. Scale bar 30 μm . * $p < 0.01$, ** $p < 0.005$ and **** $p < 0.0001$ 47

Figure 24- Cells > 20 μm recovery rate and Cells < 20 μm depletion efficiency in function to the number of cells spiked in diluted blood and 20 μm < Cells < 20 μm isolated by the device (A) schematic representation of the target cells outlets; (B) Average recovery rate and depletion efficiency of three different experiments. 50, 100, 1000 and 2000 spiked cells in the diluted blood were run into the device with 2 inlets and 2 outlets with the flow rates of sample/buffer at 100/1000 $\mu\text{L}/\text{min}$, then the recovered outlet 2 was centrifuged, reduced to 1000 μL , and run into the device with 2 inlets and 4 outlets with the flow rates of sample/buffer at 100/1000 $\mu\text{L}/\text{min}$. The depletion was measured using a ratio between the number of cells inserted in inlet less cells counted in outlets and cells inserted in inlet. Error bars represent standard deviation; Results are described as Mean +SD of 3 independent experiments (C) Cells < 20 μm pre-stained with DAPI and Cells >20 μm pre-stained with Calcein-AM recovered. Images acquired for bright field BF, DAPI Calcein-AM and merge Images obtained with the objective lens of 20x. Scale bar 30 μm . * $p < 0.01$, ** $p < 0.005$ and **** $p < 0.0001$ 49

Figure 25- Cells viability assay. After running 1000 cells pre-stained into the microfluidic system at 10 $\mu\text{L}/\text{min}$ the recovery sample was run into the device with 5 rows designed by the group. Calcein-AM cell viability assay was made to verify the viability of isolated cells. (A) Captured cells < 20 μm ; (B) captured cells > 20 μm . Images obtained with the objective lens of 20x. Scale bar 30 μm 51

Figure 26- Microscope images of the device 2 inlets/ 2 outlets channels. As observer the walls have several damages. 52

LIST OF TABLES

Table 1- Comparison between the dimensions projected in the CAD draw of the spiral devices and the PDMS microchannels. Results from a mean of 5 measurements with an optical microscope and lent of 5x and 10x..... 38

NOMENCLATURE

ADT	Androgen deprivation therapy
AJCC	American Joint Commission on Cancer
AR	Androgen receptor
BPH	Benign Pathologies
CAD	Computer-aided design
CAMLs	Cancer-Associated Macrophages like cells
CEK	CellSearch Epithelial cell kit
Ck	Cytokeratin
CLIA	Clinical Laboratory Improvement Amendments
CNC	Computer numerical controlled
CPK	CellSearch Profile cell kit
CTCs	Circulating tumor cells
DAPI	4',6-Diamidino-2-Phenylindole
Dh	Hydraulic diameter
DLD	Deterministic lateral displacement
DNA	Deoxyribonucleic acid
DRE	Digital Rectal Examination
EMT	Epithelial-to mesenchymal transition
EpCAM	Epithelial Cell Adhesion Molecule
ERG	Erythroblastosis virus E26 transformation specific related gene
FBS	Fetal Bovine Serum
FDA	US Food and Drug Administration
FDM	Fused Deposition Modelling
FISH	Fluorescence <i>in Situ</i> Hybridization
IF	Immunofluorescence
ISUP	International Society of Urological Pathology
KLK3	Prostate-specific gene kallikrein 3
LUTUS	Lower Urinary Tract Symptoms
MET	Mesenchymal-to-epithelial transition

MRI	Magnetic resonance or MR-guided biopsy
mRNAs	Messenger RNA
panCK	Pan-cytokeratin
PBS	Phosphate Buffered Saline
PCa	Prostate cancer
PCA3	Prostate Cancer Antigen 3
PDMS	Polydimethylsiloxane
PIN	Prostatic Intraepithelial Neoplasia
PFF	Pinched flow fractionation
PHI	Phosphohexose isomerase
PSA	Prostate-specific antigen
PSMA	Prostate-specific membrane antigen
RBCs	Red blood cells
Re	Reynolds number
SLA	Stereolithography
SLS	Selective laser sintering
TRUS	Transrectal Ultrasound Guided Biopsy
WBCs	White blood cells

1. STATE OF ART

1.1. Prostate Cancer

1.1.1. Epidemiology and Aetiology

Prostate cancer (PCa) is the most common, non-cutaneous male cancer remaining the second common type of cancer and the fifth leading cause of cancer-related death worldwide (1). In Portugal, PCa was the most frequent cancer among men in 2018. PCa death rates have been decreasing since the early 1990s, although rates appear to stabilise from 2013 to 2015, being the third leading cause of death among men in 2018 (Figure 1).

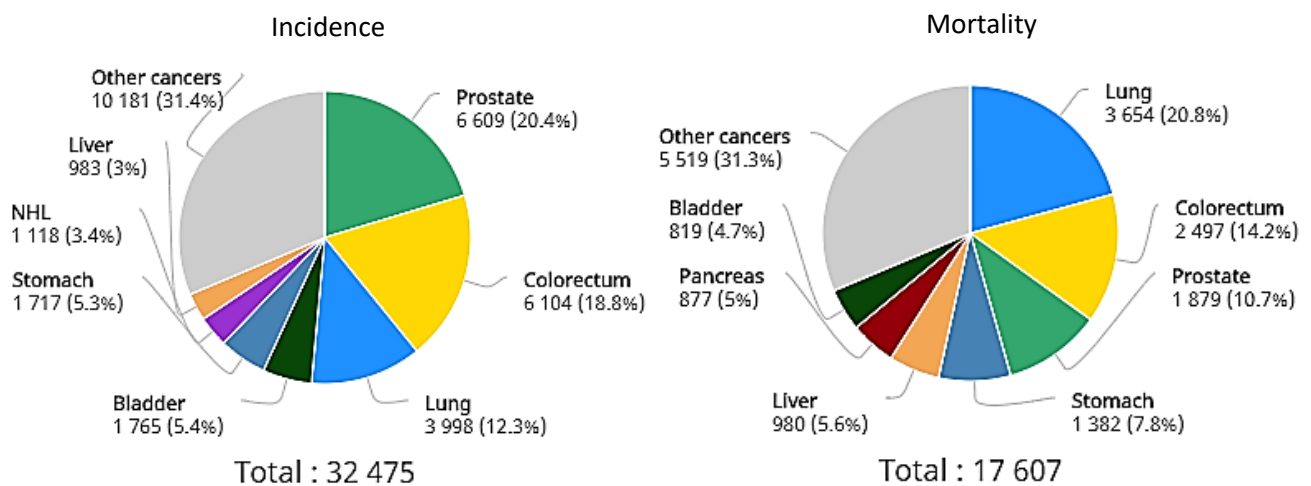


Figure 1- PCa incidence and mortality rate of the 10 most common cancers for males in Portugal 2018. Adapted from Globocan.

Significant differences in PCa incidence and mortality exist among continents, being the highest incident rates found in Oceania and North America (Figure 2). Even within a given geographical area, certain ethnic groups have a significantly higher risk of disease. The risk of developing PCa increases with age and is related to other factors such as lifestyle, nutrition, physical activity, environmental factors, and smoking (2). PCa incidence has spiked in the early 1990s due to widespread prostate-specific antigen (PSA) testing, which provided early detection and diagnostic by communities, leading to increased incidence, particularly in developed countries. (3). Limited health care services and accessibility to PSA testing in underdeveloped countries result in high mortality rates (3).

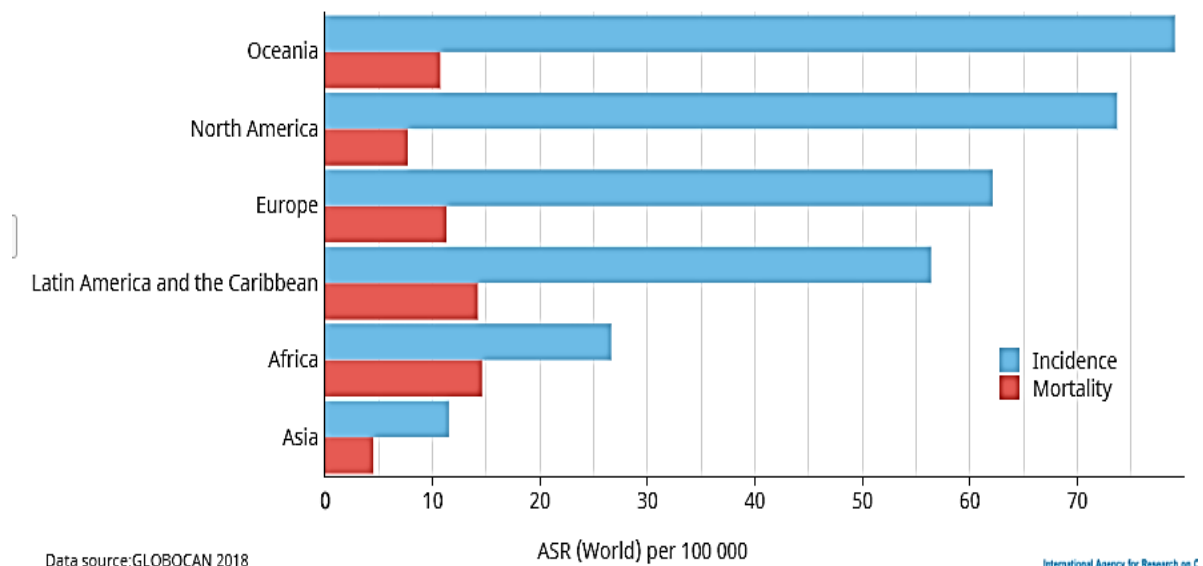


Figure 2- Estimated age-standardized incidence and mortality rates (world) in 2018, prostate, males. Adapted from Globocan.

PCa is a multifactorial disease since environmental and genetic factors, age, family health history and ethnicity may interact, favouring tumour development (2,4). Diagnoses of PCa occurs on average around 72-74 years old, with 85% of the patients being diagnosed with 65 years old or more. The majority of men above 85 years old show foci of histological PCa. Family history incidence is also a risk factor of PCa since 10-15% of all patients diagnosed with PCa have at least one relative affected. An increased number of affected family members and a greater degree of kinship increases the risk of developing PCa (5, 6). Ethnicity is also considered a risk factor for the development of PCa that justify the difference in the incidence rate of PCa worldwide (2, 5, 6).

1.1.2. Prostate Carcinogenesis

PCa is classified as adenocarcinoma, and it is further classified based on its cell of origin. The most prevalent malignant disease in prostate is developed in the acini of prostatic ducts corresponding to approximately 95% of the cases. The remaining 5% are rare histopathologic types: small cell carcinoma, mucinous carcinoma, endometrioid cancer (prostatic ductal carcinoma), transitional cell cancer, squamous cell carcinoma, basal cell carcinoma, adenoid cystic carcinoma (basaloid), signet-ring cell carcinoma and neuroendocrine cancer. The development of PCa is a multi-step process through a series of morphologically distinct lesions

Microfluidic –based isolation of rare-tumor associated cells in prostate cancer

initiated by genetic and epigenetic changes (2). From normal prostate to invasive carcinoma, three intermediate stages must be observed, namely proliferative inflammatory atrophy (PIA), low-grade prostatic intraepithelial neoplasia (PIN) and high-grade PIN (Figure 3).

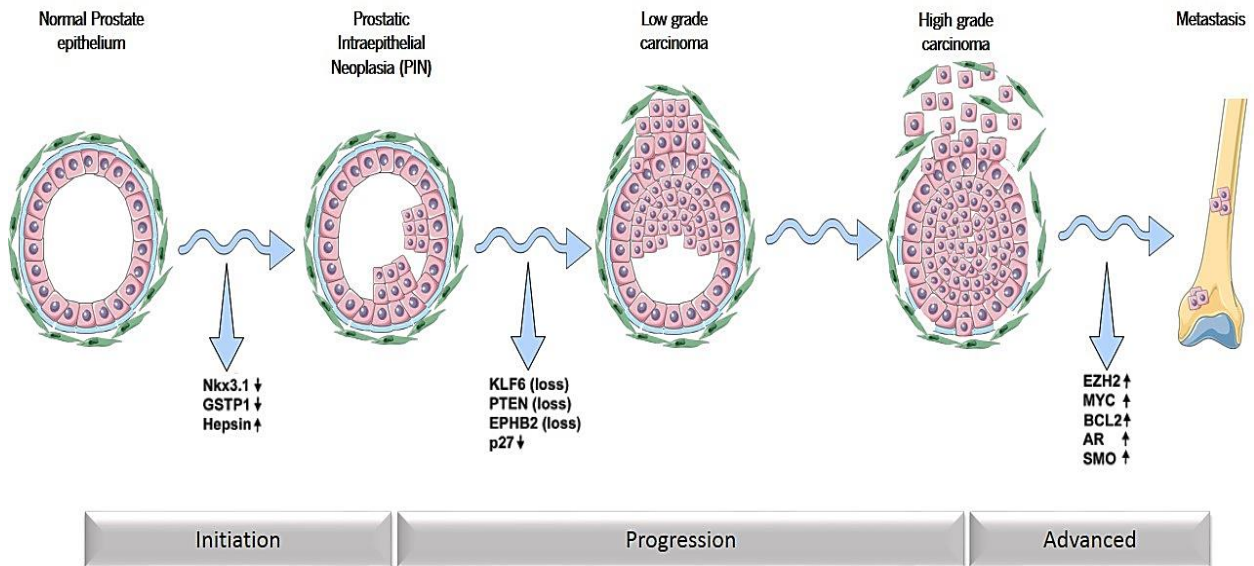


Figure 3- Prostate carcinogenesis. Morphological features of different stages of PCa progression are correlated with the molecular landscape. Prostate epithelial cells are shown in pink, the stromal cells in green and the basement membrane separating the epithelial and stromal cell compartments is shown in blue.

The normal human prostate consists of two major epithelial and stromal cell compartments. The epithelial gland comprises luminal, basal and neuroendocrine cells. The stroma consists of fibroblasts, dendritic cells, endothelial cells, mast cells, lymphocytes and nerve cells. Stromal and epithelial layers express androgen receptors (ARs), depending on androgens (i.e., testosterone) to proliferate (7, 8). When a normal prostate is exposed to infectious agents and dietary carcinogenesis, the prostate epithelium can be directly affected, resulting in PIA histological lesions. PIA usually originates in the peripheral zone and is characterized by the infiltration of lymphocytes, macrophages and neutrophils; phagocytes release reactive oxygen and nitrogen species causing DNA damage, cell injury and cell death, which increased the fraction of epithelial cells (9). PIN and PIA share similar alterations at crucial molecular pathways and originates in the same prostate glandular zone, suggesting that PIA can be a precursor of PIN (10). PIN lesions were firstly characterized by Bostwick and Brawer in *low* and *high-grade* PIN (LGPIN and HGPIN, respectively), which differ by architectural and cytological characteristics. The difference between the HGPIN and LGPIN is that the first is characterized by more crowding and stratification than the first one. HGPIN is

characterized histologically by replacing normal luminal cells with neoplastic cells that display large, hyperchromatic nuclei with prominent nucleoli (11). The basal layer may show some disruption, while in LGPIN, the basal cell layer remains intact (12). The histological changes associated with PIN are reminiscent of cancer, evidenced by the reduction of the basal cell layer, the appearance of luminal epithelial hyperplasia (7, 12). In the transition to PIN, the most notable transcription changes is upregulation of cell-surface protease hepsin (13). The final stage before the metastasis is carcinoma characterized by the loss of basal cells and marked cytological atypia characterized by nuclear and nucleoli enlargement. The basement membrane is disrupted, and tumor cells show local invasion (13). During tumor progression, the loss of the overall epithelial organization becomes more evident with tumours evolving from well-differentiated to moderately differentiated, to poorly differentiated (13). The genetic changes associated with prostate carcinoma are inactivation of the transcription factor *KLF6* and the tyrosine kinase receptor *EPHB2*, loss of the negative regulator of *PI3K* lipid phosphatase *PTEN* and downregulation of the cyclin-dependent kinase inhibitor *p27* (13). In an advanced stage of poorly differentiation, the loss of tissue organization and primary tumor invasion occurs due to downregulation of cell adhesion proteins like E-cadherin (E-cad), alpha-catenin (a-cat), CD44, KAI1, 4-integrin and basement membrane proteins laminin 5 and collagen (13). The final critical hallmark of PCa progression is the ability of prostate tumor cells to disseminate into the bone marrow and peripheral blood (13, 14). At morphological level, the cancer progression leads to an appearance of metastatic foci of PCa cells in lymph nodes and bones. Metastasis are associated with genetic changes, such as the amplification of *MYC*, the overexpression of *EZH2*, the upregulation of Smoothed (SMO), the hyperactivation of the androgen receptor (*AR*) and finally the overexpression of antiapoptotic factor *BCL2* (13).

The significant phenotypic heterogeneity, as well as the slow-growing behaviour and absence of symptoms in the early stages makes PCa a challenge concerning detection and subsequent treatment (10).

1.1.3. Diagnostic tools for prostate cancer

Since PCa is characterized by an absence of symptoms in the early stages, the majority of men with localized PCa do not have symptoms arising as a direct result of cancer itself. Almost all cases of suspected PCa are associated with lower urinary tract symptoms (LUTUS)

such as urinary frequency, urgency, decreased force of stream, and nocturia (15); other symptoms include back pain, leg swelling, peripheral neurological symptoms and new-onset erectile dysfunction (16). The current standard for diagnosis and follow-up of PCa is the digital rectal examination (DRE) and PSA blood test, followed by transrectal ultrasound (TRUS) guided biopsy (17). PSA is a glycoprotein serine protease enzyme produced by prostate epithelial cells. Physiologically, it liquefies seminal fluid. High PSA value is associated with an increased risk of PCa (16). However, in about 18% of all patients, PCa is detected by a suspect DRE, regardless of the PSA level. It can be due to low level of specificity and sensibility, leading to an overlap in PSA levels between benign pathologies (BPH) prostatitis and PCa (17). The majority of men who are detected with PCa during screening PSA program have normal DRE (16). If DRE and PSA screening results are PCa abnormal, it is recommended a TRUS. Since PCa is heterogenic, TRUS has a different sensitivity depending on where the tumor is located. Thus, TRUS is indicated for tumors located in the peripheral zone in contrast to tumors located in the transition area. Patients who have suspicions of anterior prostate cancer, with high PSA level, but who are not detected by TRUS, should be candidates for a saturation biopsy or MRI-guided biopsy (19) .

1.1.4. Molecular biomarkers

In order to improve the specificity of PCa diagnosis and reducing the unnecessary biopsies, detection of prostate cancer specific biomarkers in body fluids was implemented. Only 3 tumor marker tests have been cleared by the US Food and Drug Administration (FDA) for routine practice in patient care: PSA, Prostate Health Index (PHI) and Prostate Cancer Antigen 3 (PCA3) (20).

PSA (also Known as prostate-specific gene kallikrein 3 (KLK3), which was approved by FDA in 1994, has contributed to a significant decline (45–70 %) in age adjusted PCa mortality (20). This biomarker was rapidly adopted for early detection providing the identification of prostate diseases in conjunction with the digital rectal examination (DRE) (18,20). According to the American Cancer Society, a PSA level above 4 ng/mL has been recognized to be abnormal, and these patients are advised to undergo a biopsy (21). Since PSA is a prostate specific biomarker but not tumor-specific, PSA-based screening lacks specificity in patients

with prostatic hyperplasia, leading to over diagnosis and overtreatment of a low risk PCa (20, 22).

PHI was approved by the FDA in 2012 and consists in a mathematical formula combining all three PSA biomarkers (23). With this formula, the clinician obtained a single score for each individual making a better informed recommendation to the patient (23). This test was developed with the intent to distinguish cancerous and benign prostatic conditions in men aged ≥ 50 years old with a normal DRE and PSA levels of 4–10 ng/mL. Furthermore, several studies demonstrated the existence of a correlation between PHI scores and Gleason score ≥ 7 , which was important to reduce the number of unnecessary biopsies and a measure of cancer aggressiveness (20, 23, 24).

PCA3 is currently being tested as a urinary biomarker for PCa using DRE urine specimens. ProgenSA PCA3 assay is based on the ratio of the concentration of PCA3 RNA molecules to the concentration of PSA RNA molecules and is not affected by prostate volume or other non-cancerous prostate conditions (24, 25). PCA3 is highly expressed in around 95% of the primary and metastatic cases of PCa and is thought to be prostate-specific, as it was not detected in 18 other non-malignant tissues in a major study. In men with a high PCA3 score, the likelihood of a positive prostate biopsy is increased (20, 25, 26). Although the PCA3 has a higher specificity and better predictive value (positive and negative) when compared with PSA, in terms of sensitivity, this biomarker is lower, presenting variable values ranging from 20 to 96% depending on the threshold cut-off used for the PCA3 levels. PCA 3 has been widely studied, because of its ability to predict malignancy in men with an elevated PSA and a prior negative biopsy in order to identify men who have clinically insignificant PCa and are candidates for active surveillance (20, 25).

1.1.5. Metastization

PCa deaths are mainly related to the development of the metastatic disease, 80% of which primarily localized in the bone (27). The classic model of metastasis of solid tumors is guided by the “seed and soil” hypothesis proposed in 1889: tumors cells (“the seeds”) metastasize only to specific organ (“soil”) seeking favourable conditions for their growth and development (28). Metastasis is a complex process which involve multiple steps including cell migration, local invasion, intravasation of tumor cells into the circulation, dissemination, arrest at secondary and primary sites, extravasation into a distant site and finally formation of clinically detectable metastasis (28). Metastatic colonization depends on the so-called epithelial-to-mesenchymal transition (EMT) in which epithelial cells lose intercellular adhesion, and acquire a more motility and invasive phenotype (Figure 4) (27). After, tumor cells enter into the circulatory system as a single cell or clusters, spread to different parts of the body and infiltrate in distant organs (Circulating tumor cells (CTCs) (29). The initial arrest of CTC occurs due to the mechanical entrapment and adhesion of these cells to the vascular endothelium (30).

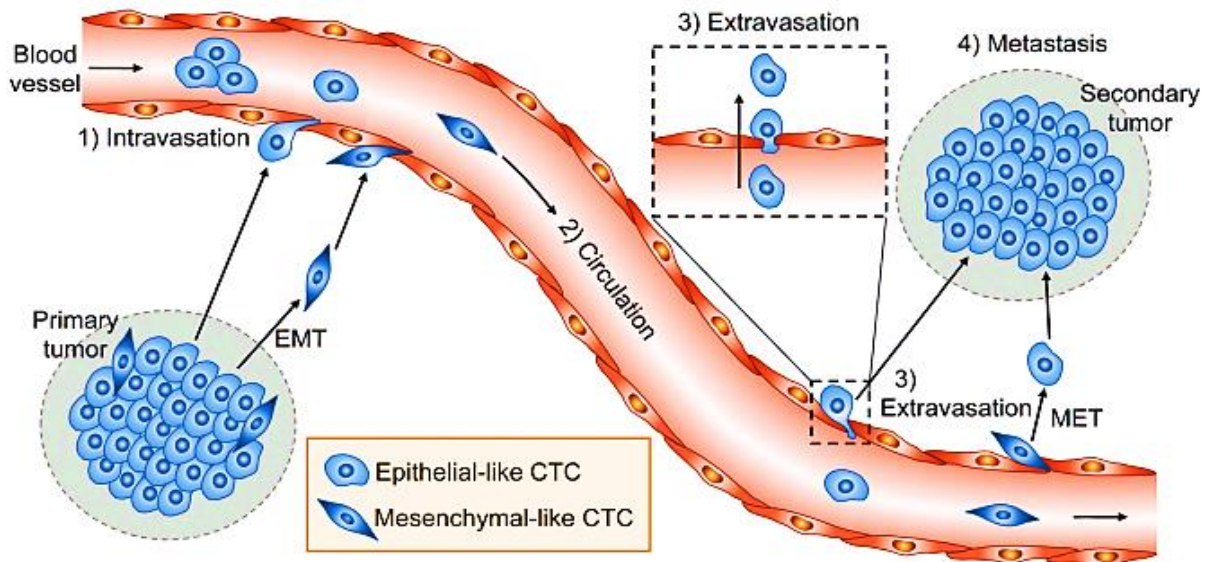


Figure 4- The role of CTCs in tumor metastasis. 1) Tumor cells enter the circulation 2) arrest of CTC in the blood stream; 3) CTC adhere to blood vessel walls and extravasate to distant sites; 4) The majority of cell die, while others enter a latent state as single cells or develop into secondary tumors. Adapted from Cho et al., 2018.

In the bloodstream, CTCs are exposed to shear stress, the innate immune system and oxidative stress, which leads to circulating tumor cells association with platelets to protect themselves (29). When subjected to the appropriate signals, cells are transitioned back to an

epithelial state, in a process named mesenchymal-to-epithelial transition (MET) (27). Subsequently, CTC begins to develop resistance to both the immune system and the defence responses of the tissue where they are found and may follow one of the three alternative pathways: cell death, begin to enter a latent state as single cells or micrometastases and colony formation by continuous proliferation. Finally, when these cells leave their latent state, they restart their growth by overcoming the microenvironment of the local tissue (30, 31).

1.1.6. Liquid Biopsies

Detection, monitoring, and molecular analyses of CTCs in a minimally invasive way using liquid biopsy have been exploited as a promising non-invasive tool towards the molecular profiling of circulating cancer-associated cells in various biological fluids, envisaging early diagnosis and real-time patient monitoring of cancer (32-34). Besides that, tumor biopsies, which are invasive and are dependent on tumor heterogeneity and genetic alterations, leads to clinical decisions based on historical biopsies. In contrast, analysis of the CTC using liquid biopsies has demonstrated promise to clinicians to allow the matching of the right drug to the right patient, contributing to personalized therapy (32). However, these rare cells' isolation is still technically challenging given their scarcity (1-10 CTCs/billion of blood cells) (33). CTC molecular expression provides essential information to classify disease phenotypic. Intracellular proteins cell surface biomarkers, including cell surface receptors, can be evaluated using immunofluorescence microscopy (IF). However, the exact identification of CTCs presents some issues due to its heterogeneity, there is no universal biomarker that can be used to classify them. The low sensitivity of methods to enumerate them also contributes to the unfixed characterization (35). Attard et al., 2011 reported expression of of CK⁺ and CD45⁺ in healthy volunteers and cancer patients, indicating that CK⁺ and CD45⁺ events are probably not associated with CTC. They explain this phenomenon through the possibility of true leukocytes ingesting epithelial cells and debris, resulting in the expression of CK antigens on their surface. Therefore, CD45⁻ represents cells that are not blood cells and CK represents epithelial cells. Finally, it was affirmed that CTC is not a CTC unless it is CD45⁻, expressing also DAPI⁺ (34). According to Si-Hong Lu et al., 2016, different types of cancer can express common markers. For better phenotypic characterization, a panel

of multiple markers is used with an accuracy of 88% and 75%. In the same study, it was verified that pan-cytokeratin (panCK) could be a good marker to distinguish cancer patients in CTC enumeration because panCK⁺ (CK 8/CK18/CK19) CTC counts were significantly higher in cancer patients than in healthy ones (36). The presented biomarkers are used to identify a CTC; however, it is impossible to predict cancer origins because a CTC is always CD45⁻ and CK18 and CK19 are useful markers and are positively expressed for carcinomas such as lung adenocarcinoma, colorectal cancer, and prostate cancer. To identification CTC origins, especially CTC for PCa patients, prostate-specific antigen (PSA) and prostate-specific membrane antigen (PSMA) have been used. PSA is commonly used for detecting metastatic prostate carcinoma, and PSMA can be expressed in neoplastic prostatic tissue (36). The combination of both is crucial because PSA alone can be expressed by breast cancer, and PSMA alone can be expressed in various tissues, such as the kidney, bladder, testis, and intestine, except for the lung and the colon. However, the positive expression of PSA/PSMA could identify PCa CTC since both expressions only occur in prostate carcinoma (32, 36).

For over a hundred years, the CTC has understandably received the most attention; however, recent studies have shown that themselves are not sufficient for the development of metastasis (37). In fact, the tumor microenvironment is composed of Leukocytes, fibroblasts, and vascular endothelial cells, being the immune cells the major component (38). These immune cells, such as monocytes and monocyte-derived macrophages, belong to the myeloid lineage of leukocytes and originate from the same progenitor cells in the bone marrow circulation can interact with tumor cell invasiveness, motility, and metastatic potential (39). Thus, when recruited into peripheral tissues from the circulation, they can differentiate in distinct, mature macrophages exerting specific immunological function (39). These specialized differentiated macrophages are called Tumor-associated macrophages (TAMs). The recruitment of monocytes into TAMs is operated by chemokines and involves various factors in the tumor microenvironment such as cytokines and growth factors (40, 41). The secretion of cytokines and growth factors by TAMs stimulate tumor cells to become into CTCs. TAMs and CTCs then migrate via the lymphatic system or intravasate across intratumor capillary barriers into peripheral circulation (42). These TAMs that have the capacity to enter in the circulation were hypothesized to be disseminated TAMs (DTAMs). Earlier in 60s some researcher showed the recovery of cells with features of malignant change from blood of

patients with cancer whereas in blood from normal controls that such cells appear rarely (43, 44). However only recently was possible to isolate and characterize them. Adams and their team term these giant cells as “Circulating Cancer-Associated Macrophages like cells” (CAMLs). These rare cells are defined as highly differentiated giant phagocytic cells of myeloid lineage. They are involved in numerous physiological and pathological processes, including phagocytosis of foreign/necrotic tissue, tissue reabsorption and inflammation (42). CAMLs are morphological heterogeneous in size ranges, shapes, and nuclear profiles. They appear very large, 25-300 μm , with large atypical nuclei (14-64 μm) or multiple individual nuclei (45). They also present morphology variants, including spindle, tadpole, round, oblong, two legs, or amorphous shapes. These cells are distinct from CTC since they are involved in phagocytosis of foreign necrotic tissue, tissue reabsorption, and inflammation (42, 46). Even though CAMLs present extreme size, large nuclear profile, and cytoplasmic signature are straightforward, they present heterogeneity and therefore presents heterogeneous markers expression (42). CAMLs express epithelial, monocyte, endothelial, and megakaryocyte protein markers and represent engulfed CTCs (47). In contrast to CTC that has been found mostly in metastatic cancers, CAMLs have been found in all cancer patients regardless of the stage (36, 46). As CTC, CAMLs molecular expression provides a more discrete identification of cancer type, especially during initial disease screening. Although the lack of knowledge on this subject, when it comes to a specific cancer origin, there are some biomarkers that are common, regardless of the cancer origin. CAMLs express CD45, CD11c, and CD14, which defines their origin as myeloid lineage, and exhibit cytoplasmic staining by cytokeratin 8, 18, and 19 and epithelial cell adhesion molecule (EpCAM) that is characteristic of epithelial cells (42, 45, 46). The degree of expression of cytokeratin, EpCAM, and CD45 can each vary from no signal to very intense expression (42). Even though some biomarkers are common, there are organ-specific markers. A previous study by Adams et al., 2014, showed the presence of PSMA⁺ debris in CAMLs from prostate samples suggesting that these cells participate in a process of phagocytosis of necrotic debris or engulfment of neoplastic cells, likely from a tumor site, as part of the innate immune recognition of and response to the tumor. PSMA is a membrane glycoprotein that is highly expressed in prostate cells. Considering the results obtained, it can be stated that CAMLs can be promising as a valid biomarker for all cancer stages (42). Adams team shows that these macrophages bound to and migrate through the circulation attached to CTCs and

promote their migration. The interaction between both may be due to two possibilities such as, the interaction occurs while in circulation, which imply that CAMLs are an active immune response to cancer cells in circulation; the second possibility refers to the possibility of these cells binding at the tumor site and disseminate together into circulation, which implies a similar pathway of intravasation (42). Although the complexity of interactions between cancer cells and innate immune cells, the characterization and monitoring of the various cellular components are indispensable to comprehends the biological characterization of solid tumors (42).

1.2. Microfluidics in cell biology

1.2.1. Technical concepts of biofluids

Microfluidics, which was introduced as a biomedical tool in the 1990s, is a technology that deals with the behaviour, precise control, and manipulation of fluids and particles on the scale of tens to hundreds of micrometres (48, 49). In contrast to conventional macro-scale platforms, this fascinating technology holds superior advantages, such as the volume of sample and reagent reduction, short processing times, enhanced sensitivity, low cost, improved portability, and allows real-time analysis and automation (48). Early cancer detection, which has been at the forefront of medical and scientific research, is crucial for improved prognosis and cancer management due to the small tumor size and localization of the tumor at the primary site (48, 49). Conventional cancer cell sorting techniques, such as centrifugation, chromatography, fluorescence, and magnetic-activated cell sorting are highly dependent upon a sampling of tumor tissues or indirect quantification of proteins (49). Besides, these conventional sampling approaches are invasive, limited in yield and purity, and further, rely on the expertise and subjective judgments of highly skilled personnel. Inherently, microfluidics is suitable for analyzing complex fluids *in vitro* and thus, offers a non-invasive alternative for cancer diagnosis and disease management (49).

To fabricate devices with clinical applications is important to take into consideration some technical concepts of biofluids. In microfluidic systems, particularly those operating with liquids, the continuum approach, which is the mechanical behaviour of materials modelled as a continuous mass rather than as discrete particles, can be considered, and the fluid is a material that can be deformed continuously under the action of shear stress (50, 51). The main

property of a fluid is the viscosity that is related to the resistance of the fluid to the deformation. In many of the fluids, the viscosity is a continuous property, varying only with pressure and temperature.

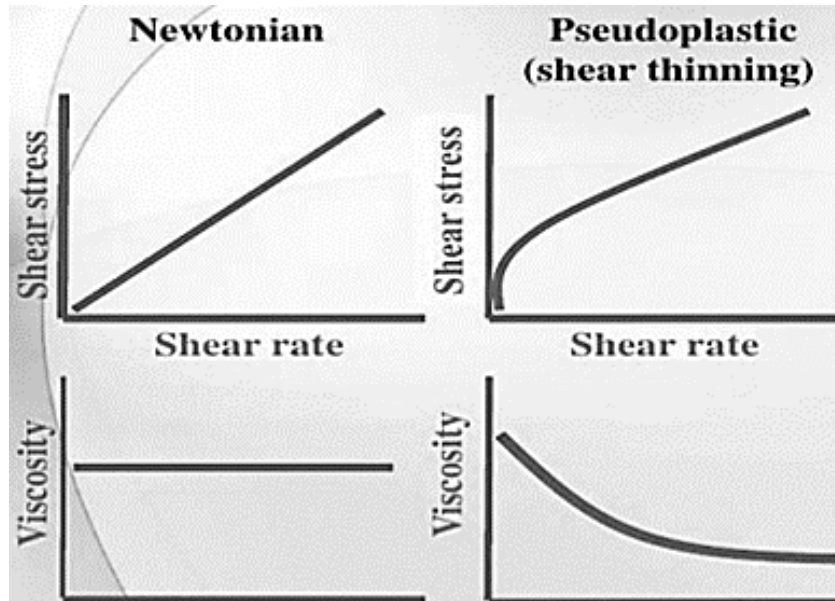


Figure 5- Variation of Shear stress and viscosity with the shear rate for a Newtonian and Pseudoplastic fluid.

For a given temperature and pressure, a fluid that keeps its viscosity constant is a Newtonian fluid (Figure 5). This fluid presents a laminar flow with a Reynolds number under 2300. A non-Newtonian fluid is a fluid that presents a dynamic viscosity behaviour given specific conditions of temperature and pressure (50, 52, 53). For example, the blood is considered a non-Newtonian fluid (pseudoplastic, shear thinning fluid) since its viscosity change with temperature and with a stress action reduce with the increase of the shear stress.

The Reynolds number (Re) consists of a ratio between inertial and viscous forces to determine if the fluid flow is laminar or turbulent, and it is a dimensionless number defined by the following equation:

$$Re = \frac{\text{inertial forces}}{\text{viscous forces}} = \frac{\rho V D}{\mu} \quad (1)$$

where ρ (Kg/ms) is the density of the fluid, V (m/s) is the average velocity of the fluid over the cross section of the tube, D (m) is the tube diameter (considering circular section) and μ

(Kg/ms) is the dynamic viscosity of the fluid (50, 52). Since most of the microfluidic devices present a rectangular section is necessary to replace the D by hydraulic diameter (D_h), which consist of:

$$D_h = \frac{4ab}{2(a+b)} = \frac{2ab}{a+b} \quad (2)$$

1.2.2. Blood Flow and its constituents

Blood is a non-homogenous fluid consisting of a suspension of cells, proteins, and ions in a viscous fluid, the plasma. The cells suspension is mainly red blood cells (RBCs), white blood cells (WBCs), and platelets. To investigate blood cells behaviour *in vitro*, the development of microfluidic devices able to mimic the microcirculatory system has been increasing. Recreate a physiologically relevant microenvironment is a critical step to modulate biochemical and biomechanical cell behaviour *in vitro* (54). Blood circulation occurs owing to the pressure gradient inside the blood vessels. As blood moves distally from the heart, the pressure drops along the blood vessels. Since RBCs occupy 45% of whole blood, the blood rheological behaviour is mostly determined by their presence (55, 56). In a macroscopic perspective, in large arteries, owing to the significant difference between the arteries and the cells diameters, the blood flow is comparable to the flow of a Newtonian homogeneous fluid. At this level, the Reynolds number is large, and because of that, the blood flow is governed by inertial forces. In microcirculation, which occurs in capillaries, arterioles, and venules, the flow behaviour is dependent on every single blood cell and its interactions. Here the Re becomes less than 1, which results in a prevalence of viscous force over inertial forces. So, to study the behaviour of blood in micro-channels is crucial to take into account the microcirculation in which non-Newtonian properties of blood are prevalent (53, 56).

1.2.3. Microfluidic technologies for cell isolation

Microfluidic systems have become increasingly used in many fields such as in engineering, biology, and medicine including blood cells separation and sorting. Moreover,

owing to their, relatively low cost and easiness of fabrication, microfluidic devices are capable of being portable and single-use, which makes them a promising tool for cell separation and for point-of-care diagnostics (57). In cell isolation devices, different cells can be sorted based on their physical and chemical properties, such as size, electrical behaviour, and chemical affinity (58). In particular, the isolation and characterization of rare cells present in blood from a cancer patient have been a promising challenging target in oncology, because its targeting and monitoring may improve the prognosis and further treatment. With this information, clinicians may apply a personalized treatment for each individual patient. In order to successfully isolate cells, there are some requirements that must be followed. Given the scarcity of rare cells and the limited sample volume to be processed, is necessary to have a high recovery rate of cells to certify that the collected ones are representative of the whole blood cells population (57). However, a high recovery does not matter if the purity is low because of the presence of other cells, the analysis step will be compromised due to that. Finally, it is important to have into account the sample throughput (57).

Typical rare cells in blood samples are circulating tumor cells (CTCs), circulating fetal cells, stem cells, and cells infected by a virus or parasite. According to the proposal of this thesis, it will be discussed only methods for CTCs and CAMLs isolation.

1.2.4. CTCs and CAMLs isolation: standard methods

To isolate CTCs from whole blood, several methods have been commonly used such as flow cytometry, immunomagnetic separation, centrifugation, and filtration. However, the CellSearch™ based on immunomagnetic cell processing has been the only system approved by FDA for CTCs capture. The CTCs are separated from the blood, when passing through a magnetic field, using anti-EpCAM antibody-coated with magnetic beads. Further, the isolated cells are analysed with fluorescent microscopy (57, 59). There exist two different kits, the CellSearch Epithelial cell kit (CEK) and the CellSearch Profile cell kit (CPK). While the first kit captures CTCs, making them permeable and labelled with DAPI, CD45, and CK and then analysed by a semiautomated counting method. The second kit isolates CTCs by using only the anti-EpCAM- based positive immunomagnetic selection. Even though the CEK is the only kit approved by the FDA, comparing with CPK, which presents a range of purity between 60-70%, the CEK has low purity, between 0.01-0.1%. Besides, the CEK is costly, time consuming,

requires extensive labour due to its immunofluorescence staining, and it implies the use of high volumes of blood (57, 59). Moreover, the CellSearch™ system presents low sensitivity, and it only detected >2 CTCs in 57% of blood patients with PCa, 37% of breast and ovarian cancer, 30% of colorectal cancer, and 26% of other cancers. This system only isolates CTCs through EpCAM labelling. Given the heterogeneity of the CTCs, the expression of EpCAM and CK vary among the different population. Given that, the system only detects CTCs from all major carcinomas. Thus it will fail to detect CTCs from other cancer typologies (59).

Another population of rare cells in blood from a cancer patient is the CAMLs, cancer associated macrophages like cells. These rare cells emerging recently in cancer studies. However, still does not exist a system approved by FDA for isolating them. Some commercially available systems, which are used for CTCs isolation can be applied to CAMLs isolation too. The number of these rare cells can be determined using a microfluidic chip based on physical size-based sorting, hydrodynamic size-based sorting, grouping, trapping, immunocapture, concentrating large cells, or eliminating small cells based on size (60). Adams et al., 2014 propose the CellSieve™ system to isolate CAMLs from peripheral blood. This method is also used to isolate CTCs. He shows that the CellSieve™ system identified at least one CTC in 72% of the patient sample and one CAMLs in 28 blood samples of 29 samples tested, while CellSearch™ identifies at least one CTC in 58% of samples. Further, CellSieve™ is a low-pressure microfiltration assay and, in contrast to CellSearch™, which uses EpCAM antibodies to enrich the CTC, it isolates CTCs and CAMLs by size exclusion (42). The low pressure applied does not damage the cells, allowing for histological identification for cellular morphology (60). Besides, CellSieve™ is constituted with precision, transparent and nonfluorescent microfilters with precision pores size and pores distribution, which turns it ideal for microscopy imaging analysis and provides a high capture efficiency. Nevertheless, the most common fabrication method, the track etch method, has randomly located pores that overlap what might leads to the looseness of some CAMLs and CTCs (60, 61).

1.2.5. Label-free cell isolation: microfluidic technologies

In contrast to the standard separation methodologies, which are based on targeting specific biomarkers to isolate the cells, the microfluidic devices isolate cells combining non-traditional biomarkers and intrinsic cell properties, such as size, density, shape, electrical

polarizability, deformability, compressibility, and hydrodynamic properties (57). Thus, these microfluidics isolation methods can be classified as passive (also known as label-free), active, or hybrid methods (Figure 6). The first ones whose methods are based on physical properties are not reliant on any external forces. The cell separation occurs through channel geometry due to intrinsic hydrodynamic phenomena such as pinched flow fractionation (PFF), deterministic lateral displacement (DLD), inertial forces, and intrinsic physical property of cell (57, 62). Although the active methods require laboratory setups more complicated, the force manipulation occurs easily. So, it does not imply the use of a new device every time a new application is desired. The hybrid methods (Figure 6) consist of a combination of the advantages of both active and passive to achieve higher requirements for performance, versatility, and convenience.

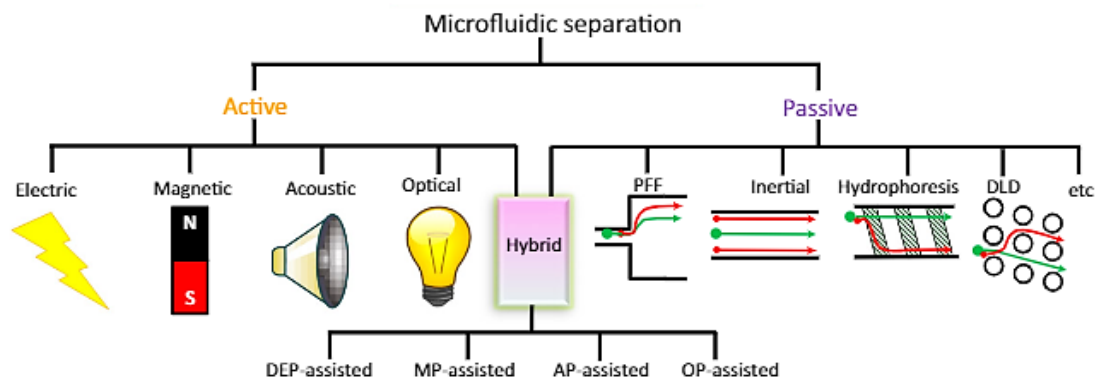


Figure 6- Classification of microfluidics isolation methods. Adapted from Yan et al., 2017.

To achieve the best performance of microfluidic devices is important a compromise between some parameters and the intended downstream application. These parameters include capture efficiency/recovery rate, purity, cell viability, processing speed, sample preprocessing requirements, cost of consumables and equipment, repeatability, and reliability.

Size-based passive filtration is the most explored technique to isolate CTCs, once these cells present a diameter significantly greater than the residual blood cell (57). CTCs diameter varies from 15 to 25 μm while RBCs present diameter of 7-9 μm and leukocytes (WBCs) that include granulocytes, lymphocytes, and monocytes present diameter of 8–15 μm , 5.2–10.5 μm , and 9.7–10.5 μm respectively (62, 63). This technique, which is simpler, and provides high throughput and high isolation performance, exploits uniform and precise microfilters in the form of pores, cavities, and other geometric barriers such as dams and pillars (62, 63). Thus,

as CTCs are larger than the other blood cells, on the flow of blood through microfilters, these rare cells are captured while the smaller-size RBCs, WBCs, and platelets can easily pass through (62, 63). Even though microfilters allow the precise adjustment of the filter pore size, they need to overcome different barriers, such as clogging and absorption on filter surfaces, which would eventually affect the cell isolation efficiency (62, 63). One way to minimize such a problem is by using higher fluid driving forces. However, it can damage the cells by affecting the viability (62, 63).

Pinched flow fractionation (PFF) is a continuous size-separation technique that benefits from laminar flow characteristics for ordering the cells based on their size for the subsequent sorting (63, 64). This technique is based on the introduction of two fluids: one containing the particles that will be sorted and the other one free of particles (63, 64). The solution of both inlets will cross at a narrow channel called the pinched segment (63, 64). The particles then get toward the channel sidewall such that the centerlines of the particles of different sizes will be positioned in different streamlines in the pinched segment. Due to the laminar nature of the flow, the particles follow streamlines according to their centre of mass (63, 64). Bodmer W et al., 2015 applied this method to isolated CTCs from WBCs, obtaining efficiencies over 90%. With this proposed device they show that the high shear rate combined with the corner effect in PFF devices may be the reason for the improved separation of cancer cells and WBCs. They also demonstrated that increasing the sample flow rate to decrease the time for all sample processing did not affect the cancer cells recovery, whereas the WBC removal decreased. Thus, further investigations are needed to avoid the decrease in WBC removal (65).

Deterministic Lateral Displacement (DLD) is often used in studies that explore microfluidics for the recovery of the tumor cells spiked in blood were in high yields (66). This technique allows the separation of particles based on their size, deformability, and shape due to micro post arrays arranged in rows, where each row has a lateral offset from the previous (57, 63). In the DLD method, control over sorting is given by the design of the array features. Thus, particles below a critical diameter flow a fluid trajectory without experiencing any lateral displacement, while particles with size over the critical diameter will be displaced laterally due to the collisions with the obstacles in each row as they advance as depicted (57, 63, 66). Liu et al., 2013 developed a microfluidic chip for the continuously high throughput processing of

whole blood with efficient isolation of cancer cells using DLD structure. It was reported that this device presents a recovery of 99% and 80% for MCF-7 and MDAMB231, respectively. Comparing to current technologies for CTC enrichment, this device presents a significantly higher throughput, which allows the combination with other techniques, such as antibody based immune-binding methods for post-capture processing (67).

Recently high-throughput passive particle sorting based on the inertial migration of particles inside curvilinear microchannels has been reported. Dean flow fractionation (DFF) utilizes the interplay between the inertial lift forces and the effects due to the action of centrifugal forces to separate particles based on their size in curved microchannels. In microchannels, due to the parabolic velocity profile, the fluid in the center experiences a higher centrifugal force than the one in the walls (63). By selecting the appropriate channel dimensions such that the larger CTCs undergo inertial focusing, while the migration of the smaller hematologic cells (RBCs and leukocytes) is solely affected by the Dean drag, we can effectively isolate CTCs from the blood (68). The major advantages of this isolation method are that it does not require any integration of external force fields, allows continuous separation without any clogging issues with extremely high throughput and efficiency, and allows the customization of the device dimensions for isolating other rare-cells from the blood (69). Khoo et al., 2014 developed a three-layered spiral device, which combines inertial and hydrodynamic Dean Forces. It was reported that this device presents a recovery of 85% of spiked cells from various cancer cell lines and 99% depletion of WBCs in whole blood at a high rate. This device detects more CTC comparing with the CellSearch™ system. However, it is necessary additional preparatory steps such as remove platelets and RBCs debris, which dilutes CTCs in large volumes. To overcome this issue is necessary an additional concentration step before analysing what can lead to information loss. Despite that, the concept has been successfully applied, and the chip denoted as CTCchip® FR1 is the key element of the commercially available ClearCell®FX1 system (57, 59, 70).

Regarding CAMLs, despite the conventional methods, there are no microfluidic approaches to isolate them from whole blood. However, given their large size (25-300 µm) and active labelling due to their CD45 positivity and EpCAM expression, the combination of both physical properties and labelling expression can form a unique profile for multiple cell separation.

Thus, using microfluidic devices allows efficient research for CTC detection and analysis because of their bio-mimicking capability, miniaturized geometric properties, and reproducibility. Besides that, the use of microfluidics to isolate CAMLs could be applied and developed, which will improve the earlier cancer diagnostic and consequently cancer therapy.

1.2.6. Fabrication of microfluidic systems

In microfluidics fabrication, it is important to have into consideration the fabrication method and the properties of the material that will be used. Therefore, to choose the appropriate fabrication method is important to evaluate technologies and equipment availability, the cost, the speed, and the fabrication capabilities (e.g., desired feature size and profile). Concerning the properties of the material, there are some, such as mechanical strength, thermal stability, chemical inertness, optical transmission, electrical insulation, and dielectric and surface properties that must be considered (71-73).

Much of the work in the field of microfluidics was performed using soft lithography. This technique introduced by Whitesides in 1998 encompasses replica molding using an elastomeric material, specifically polydimethylsiloxane (PDMS), for the fabrication of microfluidic devices, as well as for the patterning of surfaces using PDMS stamps. Soft lithography is a fundamental low-cost technique, which involves two main processes: photolithography mould processing and second PDMS processing. The photolithography for the moulding process (Figure 7) starts using an irradiation source and a photosensitive polymer to perform the pattern transfer to a silicon wafer. A photomask is necessary to control the light that is used to induce chemical reactions in a photosensitive thin film, a photoresist. The exposed thin films to UV light are chemically treated to dissolve the exposed areas (positive photoresist) or the unexposed areas (negative photoresist). The photoresist works as a mask to selectively etch the silicon wafer. At the end of the process, it is removed, leaving the pattern (74, 75).

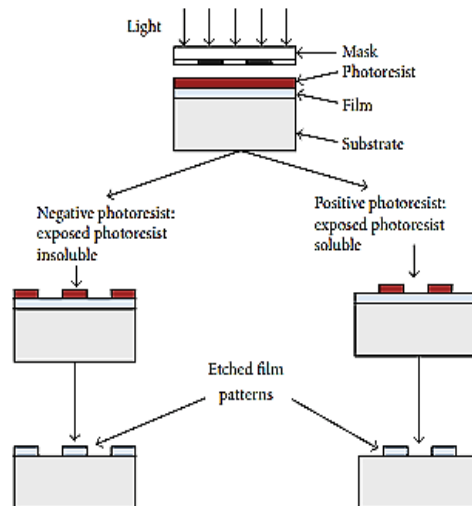


Figure 7- Photolithography steps with positive and negative photoresist. Adapted from Bellah et al., 2012.

The SU-8 photolithography method is the most common moulding media used for PDMS based microfluidic structure fabrication. SU-8 is a negative photoresist and, when exposed to the radiation, the exposed areas become rigid and insoluble, while the non-exposed areas are removed. This results in high mechanical and thermally stable lithographic structures after processing (74). After the moulding process, the master is exposed to a surface chemical treatment, named silanization, to increase the moulds durability and reduce the PDMS adhesion to the pattern structures. PDMS processing (Figure 8) is the second step to obtain microfluidic devices. Polydimethylsiloxane has several attractive properties: it is inexpensive when compared with silicon or glass; its moulding process is safe and easy to learn; it is optically transparent, and gas and vapour permeable. These properties make it suitable as a material for rapid prototyping of microfluidic devices capable of supporting a wide range of applications (74, 76, 77). After the moulding process and silanization, PDMS is cast over the master and cured. After that, the PDMS stamp is ready to be peeled.

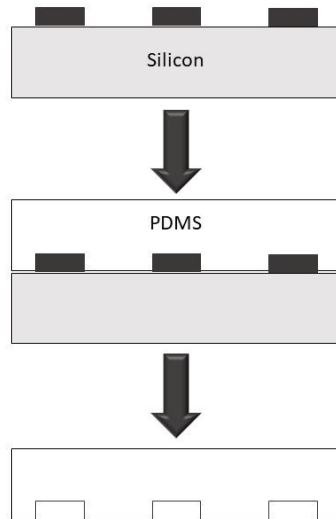


Figure 8- Soft lithography to fabricate microfluidic devices in PDMS. Adapted from Faustino et al., 2015.

Bonding the PDMS layer with the patterned geometries to a slide glass or other materials (PDMS, acrylic, among others) is the next step to achieve a microfluidic device for biomedical application. For the bounding to occur is necessary to produce strong and conformal bonds between materials surfaces. The most common method used for irreversible bonding is the oxygen plasma activation (78, 79). In plasma treatment, some parameters can affect the proper adhesion, such as power, oxygen flow, and plasma exposure time. Each factor depends on the desired application and design of the microfluidic platform. For instance, higher exposure time and higher power lead to the formation of bulking instabilities and, consequently, lead to an increase of surface roughness and a decrease of the effective contact area, and therefore the bonding efficiency stays compromised (78, 79). Besides the soft lithography procedure, other alternative fabrication methods can be used. One of those is the micromilling, which consists of the creation of microstructures via cutting tools that remove bulk material following the next steps: layout design using a software CAD, high precision computer numerical controlled (CNC) milling, and debris removal. This technique does not require a clean-room environment and specialized equipment, which can be quite costly and time consuming. Milling fabrication uses a high-speed spindle with rotational speed and micromills tools where the cutting edge can have dimensions smaller than 100 μm

(80, 81). Moreover, 3D printing has been reported as a promising alternative to traditional methods for microfluidic device fabrication. 3D printing consists of a layer-by-layer manufacturing method, which allows print complex structures from the digital designs, avoiding multi-step processing (82, 83). This technique can be carried out in our laboratory, which provides a lot of advantages such as accessibility, low cost, high efficiency, and versatility and reduces outsourcing processing time. However, some challenges need to be studied. The accuracy and the material, which will be used are the main problems of this technique (82, 83). To choose the appropriate commercial 3D printer for fabricating microfluidic devices, several considerations are necessary to have into consideration, such as the resolution, processing time, and printing dimensions. The main 3D printing methods are stereolithography (SLA), Fused Deposition Modelling (FDM), selective laser sintering (SLS), and direct ink writing (inkjet). FDM is the most used 3D printing method in microfluidics fabrication because it is the most simple and low-cost 3D printing method (82, 83).

1.3. Aims

Prostate cancer (PCa) is the most common neoplasia among men. Liquid biopsy has recently been exploited as a promising non-invasive tool towards the molecular profiling of circulating cancer-associated cells in various biological fluids, envisaging early diagnosis and real-time patient monitoring of cancer. Among those cells, circulating tumour cells (CTCs), released from the primary tumour into the bloodstream, are considered the leading promoters of metastasis. Another atypical cell population identified in peripheral blood of PCa patients is the cancer-associated macrophages-like cells (CAMLs) that have been reported to interact with CTCs, hitting a role for CAMLs in cancer cell dissemination. Efficient technologies able to isolate and detect all CTC subpopulations and CAMLs are urgently required.

Taking this into account, the main goal of this work was to efficiently isolate CTCs and CAMLs from the blood of PCa patients.

To accomplish this goal, we attempted the following specific aims:

1. To design and develop microfabricated cell capture devices.
2. To generate *in vitro* giant cells from human monocytes to mimic the CAMLs in the optimization step.
3. To optimize the flow rates for the microfluidic system
4. To isolate giant cells and deplete PCa cells (DU-145) in the microfluidic system.

2. MATERIALS AND METHODS

2.1. Cell culture

Human prostate cancer (PCa) cell line DU-145 was cultured in RPMI 1640 medium (Gibco) supplemented with 10% (v/v) fetal bovine serum (Gibco, Invitrogen) and 1% of penicillin-streptomycin (Gibco, Invitrogen). Cells were maintained at 37°C in an atmosphere of 5% CO₂ until confluence. These cells were obtained from the Leibniz Institute DSMZ-German Collection of Microorganisms and Cell Cultures Gmb (Germany), tested and authenticated. Cells were monitored by microscopy and tested for mycoplasma contamination.

2.2. Isolation and culture of monocytes

Buffy coats of healthy donors were obtained from the Hospital of Braga, Portugal, and subjected to monocytes isolation procedure using the RosetteSep™ human monocyte enrichment cocktail kit (StemCell, Cambridge, MA), according to the manufacturer's instructions (Figure 9). This study was approved by the committee of Hospital de Braga and Clinical Academic Center- 2CABraga.

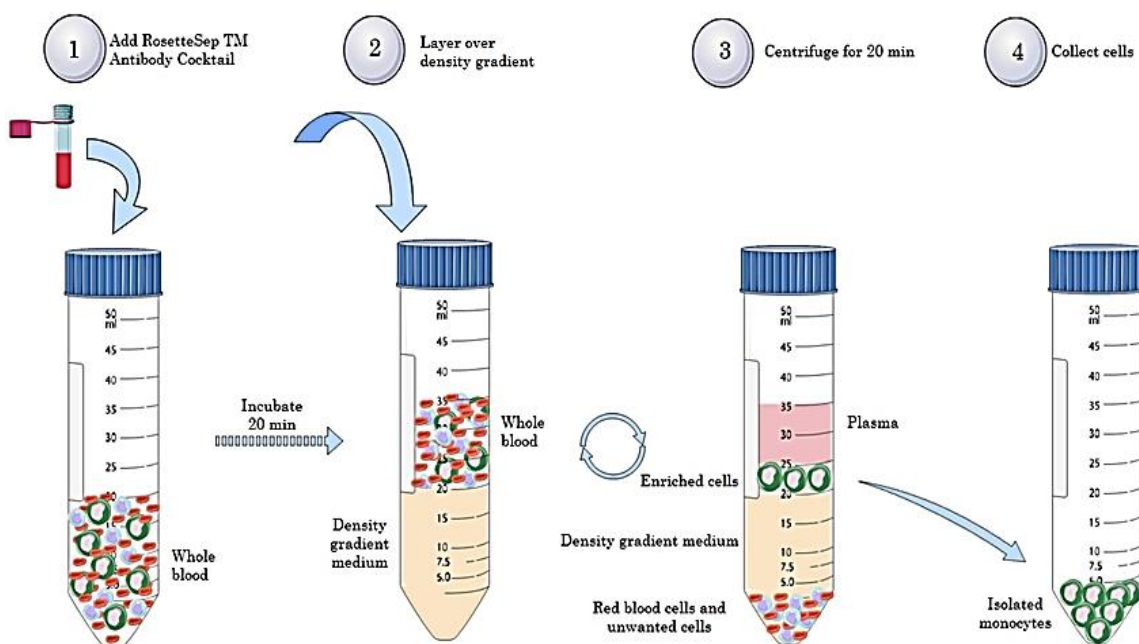


Figure 9- Manufactures guidelines for the use of RosetteSep™ human monocyte enrichment cocktail kit.1- add Rosette Antibody cocktail; 2- layer the diluted blood over density gradient; 3- centrifuge for 20 min to separate the enriched cells; 4- collect the layer with the monocytes.

Microfluidic –based isolation of rare-tumor associated cells in prostate cancer

First, buffy coats were centrifuged for 20 minutes at 120g with centrifuge break off to remove plasma (Figure 10 (A)). Samples were then incubated with RosetteSep™ Cocktail (50 μ L per 1 mL of sample) for 20 minutes at room temperature. After, samples were diluted in phosphate-buffered saline (PBS) + 2% of fetal bovine serum (FBS) and gently layered on top of histopaque-1077 (Sigma-Aldrich) density gradient medium and centrifuged for 20 minutes at 1200xg with break off and at room temperature. It is important to ensure that the blood did not mix with the density gradient medium. After centrifugation, the monocytes-enriched layer will appear at the interface between the histopaque medium and diluted plasma (Figure 10 (B)). Monocytes were then collected and washed twice with PBS + 2% FBS. If red blood cells (RBCs) were observed, samples were incubated with ACK Lysing Buffer (Gibco, Invitrogen) for 2 minutes at room temperature and washed twice with PBS + 2% FBS. Monocytes were counted with trypan blue (Sigma) and seeded (5×10^5 per well) in a 24-well culture plate in RPMI + 25% FBS + 1% penicillin-streptomycin and cultured during 48 hours to promote their adhesion before treatment.

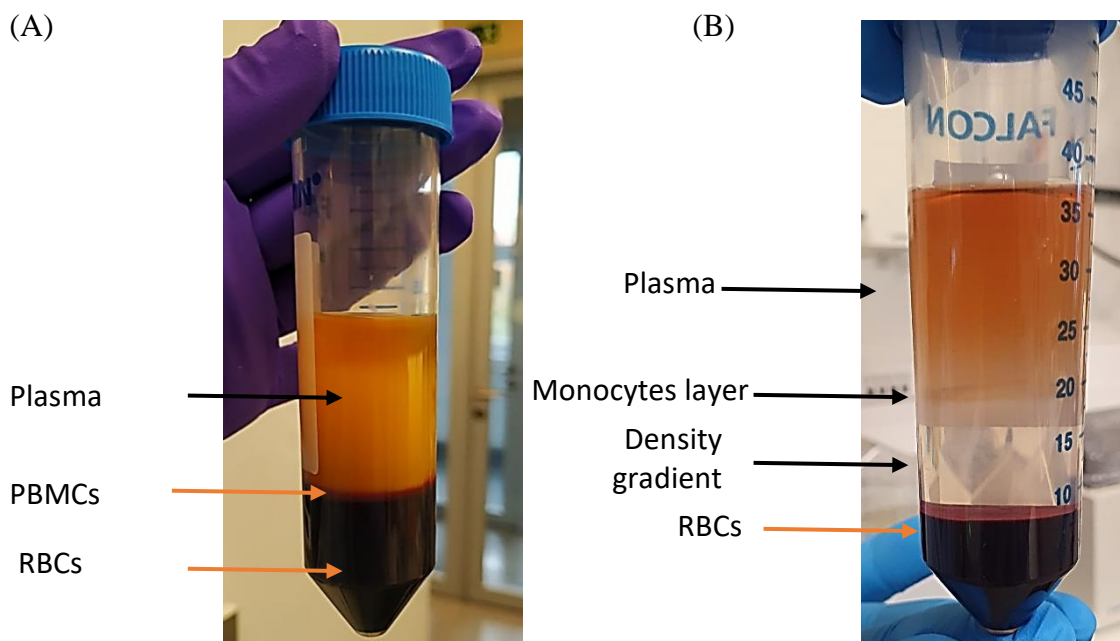


Figure 10- Monocytes isolation. (A) Layers resulted from first centrifugation in order to remove the plasma (B) layers resulted from density gradient centrifugation of sample.

2.3. *In vitro* generation of giant cells

After 24 hours of isolation and further seeding, culture medium containing non-adhered monocytes was centrifuged and monocytes added to the wells in fresh RPMI medium with 25% FBS + 1% penicillin-streptomycin. At day two of culture, and to promote the generation of giant cells, adhered monocytes were treated with the following cytokines during 10 days: IL-4 (10ng/mL); IL-4 + IL-3 (10ng/mL each); IL-4 + GM-CSF (10ng/mL and 5ng/mL, respectively); IFN- γ (100U/mL); IFN- γ + IL-3 (100U/mL and 10ng/mL, respectively), and IFN- γ + GM-CSF (100U/mL and 5ng/mL, respectively), in RPMI + 25% FBS + 1% penicillin-streptomycin. Alternatively, after isolation, monocytes were seeded in 24-well plate in RPMI + 25% FBS + 1% penicillin-streptomycin supplemented with Human Macrophage Colony Stimulating Factor (hM-CSF, 50ng/mL), and after five days the adhered monocytes were cultured with medium supplemented with hM-CSF (50ng/mL) + IFN- γ (100U/mL) + IL-3 (10ng/mL) cytokines for additional 10 days. Every two days, the culture medium was removed and replaced with a fresh one. In control experiments, cells were cultured with only RPMI + 25% FBS + 1% penicillin-streptomycin. All the recombinant cytokines were purchased from Immunotools and PeproTech.

Cells were daily checked for clustering and fusion by using a Nikon Eclipse TS100 microscope. After ten days of treatment with cytokines, giant cells were detached with a cell scraper and were collected to further microfluidic experiments. At the endpoint, the area of at least 30 adhered and detached giant cells were measured by using the ImageJ software.

2.4. Design considerations of microfluidic devices

Our team has designed two microfluidic devices by using AutoCAD software to efficiently isolate two distinct populations of rare blood cells: CTCs and CAMLs. Such design is based on the Dean Flow Fractionation (DFF) method. DFF consists of an inertial microfluidic-based sorting method in which cells/particles flowing through a spiral microchannel can migrate across streamlines by following two different rotating vortices known as Dean vortices in the top and bottom of the channel (Figure 11) (84-86).

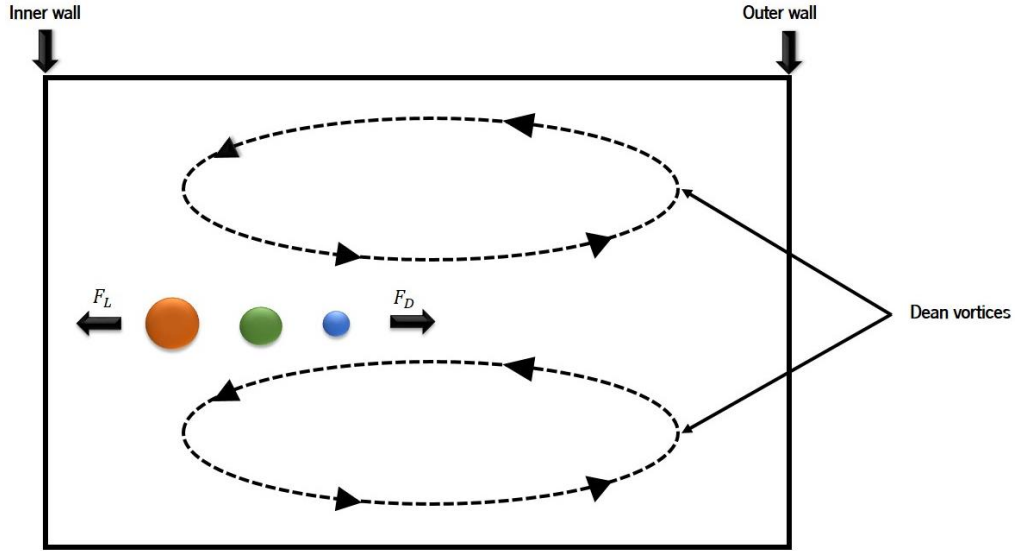


Figure 11- Schematic cross section of a curved microchannel, illustrating the focusing positions of particles of varied size. The lift force and the Dean Drag force are highlighted.

The magnitude of the Dean vortices is quantified by an adimensional parameter, the Dean number (De) given by equation 3:

$$De = \frac{\rho U_F D_H}{\mu} \sqrt{\frac{D_H}{2R_C}} = Re \sqrt{\frac{D_H}{2R_C}} \quad (3)$$

where ρ is the fluid density, U_F is the average flow velocity, μ is the viscosity of the fluid, R_C is the radius of curvature of the path of the channel, D_H is the channel hydraulic diameter and Re is the flow Reynolds number (ratio of inertial to viscous force) (84-86). The Dean vortices will also impose additional lateral Dean Drag force (F_D) on the cells/particles, represented by Stokes' law (equation 4):

$$F_D = 3\pi\mu U_{Dean} a_c \quad (4)$$

Depending on the size of the particles/cells, the drag force causes particles to move towards the inner or outer channel wall (84-86), that together with the Dean drag force, the particles will flow in an equilibrium position in a curvilinear channel. The equilibrium position is affected by the channel dimension allowing the possibility to design the spiral channel to focus only the larger target particles and cells near the inner wall while leaving the smaller unwanted particles and cells dispersed and following the streamlines (84-86). Combining the

Microfluidic –based isolation of rare-tumor associated cells in prostate cancer

advantages of Dean migration and inertial focusing, it is possible to separate particles and cell mixtures of varying sizes (84, 85).

Since CTCs and CAMLs differ in their size, a size threshold must be set for the channels to extract the target cells appropriately. Although some researches have demonstrated the possibility of such device configuration for CTC isolation directly from whole blood, the considerable contamination from red blood cells and WBCs compromises its outcome (84-86). Thus, two different spiral devices were fabricated, one with two outlets for a first separation step, in which a separation of cells under $20\ \mu\text{m}$ from cells over that target size occurs, and a second device with four outlets to separate the desired populations individually, i.e., CTCs from CAMLs and possible contamination of RBCs and WBCs. The size threshold of $20\ \mu\text{m}$ was defined for both microfluidic devices because all CAMLs and most CTCs are cells with a diameter over $20\ \mu\text{m}$. Thus, the target cells are separated by their size, while non-target cells are depleted by the waste (outlet 1). The specific design used for the fabrication of the spiral devices is available in Figure 12.

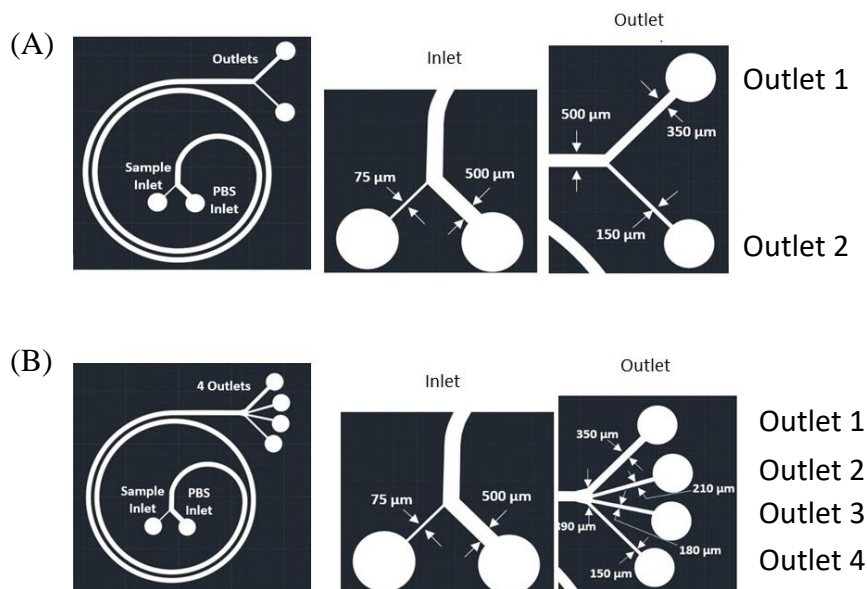


Figure 12- Design in AutoCAD software with the respective lengths of inlets and outlets (A) device with two inlets and two outlets; (B) device with two inlets and four outlets.

Both devices present a two-loop spiral channel of 500 μm of width and a depth of 170 μm . The inlets are equal for both, composed of two inlet channels with 75 and 500 μm width, respectively, the sample and the buffer inlet (see Figure 12). Near the outlet region, the channel gradually expands to a larger width that bifurcates into the outlets with different widths. Thus, the spiral device with two outlets presents 350 μm (outlet 1) and 150 μm (outlet 2). The one with a four outlets design has respectively 350 μm (outlet 1), 210 μm (outlet), 180 μm (outlet 3) and 150 μm (outlet 4). With the relation of these dimensions and microchannel depth, it is possible to achieve the isolation size threshold of 20 μm , as proposed by Warkiani et al., 2015 (86).

2.5. Fabrication of the microfluidic devices

After the microfluidic devices' design, described in the previous section, moulds were manufactured by photolithography technique (Figure 13). An ultra-thick layer of photoresist (AZP4110) was spin-coated onto the silicon (Si) wafer and patterned by direct UV exposure using a DWL machine. Further steps of resist development and etching were performed until the achievement of the final mould.



Figure 13- Silicon wafer with the devices moulds fabricated by photolithography: (A) device with two inlets and two outlets; (B) device with two inlets and four outlets.

After the photolithography process, moulds were silanized with few drops of trichlorosilane (tridecofluoro-1, 1, 2, 2-tetrahydrooctyl-1-trichlorosilane) (97%, Sigma Aldrich) for 20 minutes to improve her lifetime and to help with the polydimethylsiloxane (PDMS) detachment.

Devices were fabricated in PDMS (Sylgard 184 Silicon Elastomer kit, Dow Corning), which was prepared as a two-part system with a mix ratio of 10:1 (w/w) base/curing agent, and poured over the silicon wafer with the moulds, degassed, and cured for 2 hours at 65°C. Following that, the PDMS was un moulded, and inlets and outlets ports were made using a 1.5 mm puncher (Kai Medical). Any PDMS debris on the devices replicas was removed to ensure the proper bounding with the glass surface. Afterwards, irreversible bounding was achieved through surface activation of clean glass slides and PDMS replicas by exposure to an oxygen plasma environment into a plasma cleaner's chamber (Harrick Plasma). Then the bounding surfaces of the glass slide and PDMS replica were brought into contact. To reinforce the bounding, the devices were placed at 65°C for 30 minutes.

2.6. Set up preparation of microfluidic system

Two syringe pumps (Harvard and SPLab02) were used to generate continuous and stable flow in the fabricated PDMS devices. Pumps were firstly calibrated with the brand and volume of the syringe to be used. After, syringes (Terumo) were connected to the inlets for the sample and buffer injection using EVA plastic tubing (ID 0.5 mm, OD 1.5 mm) with 25 cm of length, needles, and tips. The outlets were also connected to the recover reservoirs (15 mL falcon tubes) with EVA tubing, with 15 cm in length. After all the connections performed, devices priming and sterilisation were performed. Firstly 70% (vol/vol) ethanol was injected into the spiral chip at an appropriate flow rate (500 μ L/min) for 5 minutes to sterilize the system and to get rid of bubbles, follow by PBS for 3 minutes at 500 μ L/min to wash the residual ethanol from the system. A filtered sample of Pluronic F-127 (Sigma Aldrich) at 1% (w/v) in PBS was then passed through the devices at the flow rate of 250 μ L/min for 5 minutes, wait for 3 to 5 minutes and finally, PBS was again injected to clean any residual of Pluronic solution.

2.7. Flow rates optimization

The microfluidic-based isolation devices' performance was performed by using DU-145 cells (that will represent CTCs) or giant cells (representing CAMLs) suspended in 1.5 mL of PBS. DU-145 cells were obtained by trypsinization using 10% (v/v) of 0.25% Trypsin-EDTA (1X) (Gibco), and the giant cells were detached using a cell scraper. The prepared sample and the buffer (PBS) were injected into the microfluidic devices at different flow rates: 100 or 200 $\mu\text{L}/\text{min}$ for sample; 600, 800, 1000, and 1200 $\mu\text{L}/\text{min}$ for buffer for the device two inlets/two outlets; and 500, 600, 800, 1000 and 1200 $\mu\text{L}/\text{min}$ for buffer for the device two inlets/four outlets. After running, outlets samples were collected, centrifuged at 1200 rpm for 5 minutes, and the pellet re-suspended in 1000 μL of PBS. 50 μL of the final volume of each was considered for counting isolated cells by using Turk solution. The system efficiency was evaluated by obtaining the ratio between the number of cells in the interest outlets over the total number of cells recovered in all outlets.

2.8. Spiking Experiments

To evaluate the efficiency of the devices to isolate cancer and giant cells, DU-145 prostate cancer cells and/ or giant cells (2000, 1000, 100, and 50 cells) were firstly stained with nuclei or viability markers (DAPI, 1mg/mL and Calcein-AM, 12.5 $\mu\text{g}/\text{mL}$, respectively, Sigma-Aldrich). Pre-labelled cells were then spiked in diluted whole blood (1:3 in PBS), and the cell suspension was then processed through the microfluidic device with two inlets and two outlets at 100 $\mu\text{L}/\text{min}$, and buffer at 1000 $\mu\text{L}/\text{min}$. Outlet 2 was recovered, centrifuged at 1200 rpm for 5 minutes, and pellet reduced to 1000 μL . This later cell suspension was then processed through the microfluidic device with two inlets and four outlets at 100 $\mu\text{L}/\text{min}$, and buffer at 1000 $\mu\text{L}/\text{min}$. The four outlets of that device were recovered separately, centrifuged at 1200 rpm for 5 minutes, reduced to 500 μL , and plated in 48 well-plate for microscope visualization and counted the number of labelled cells. An inverted fluorescence microscope (Nikon Eclipse Ti) was used. Figure 14 illustrates a schematic representation of these spiking experiences.

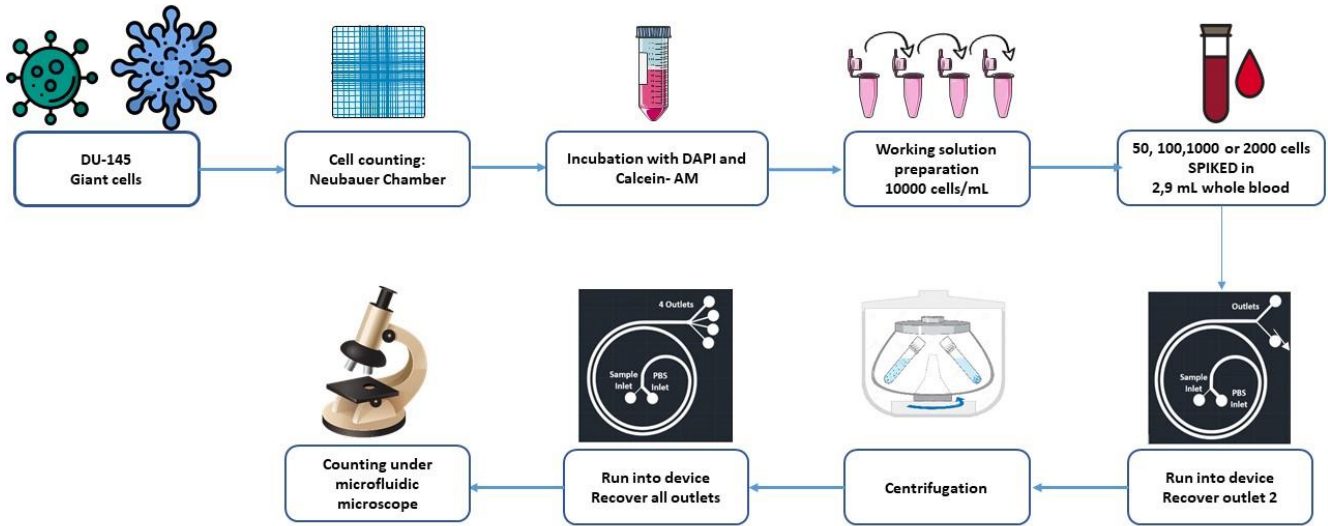


Figure 14- Schematic representation of the spiking experiments: 50, 100, 1000, and 2000 DU-145 or giant cells pre-stained with DAPI and Calcein-AM were spiked in the diluted blood and run into the device with two inlets and two outlets with the flow rates of sample/buffer at 100/1000 $\mu\text{L}/\text{min}$, then the recovered outlet 2 was centrifuged, reduced to 1000 μL and run into the device with two inlets and four outlets with the flow rates of sample/buffer at 100/1000 $\mu\text{L}/\text{min}$. The cells obtained in each outlet were counted under fluorescence microscope.

2.9. Analysis of cells isolation

Isolation efficiency of the devices, purity of the samples recovery and the depletion of cells under 20 μm , for the spiking experiments, were determined by the following equations 5, 6 and 7, respectively.

$$\text{Isolation efficiency (\%)} = \frac{n^{\circ} \text{ of isolated cells}}{n^{\circ} \text{ of cells in inlet}} \times 100 \quad (5)$$

$$\text{Purity (\%)} = \frac{n^{\circ} \text{ of isolated cells} > 20\mu\text{m}}{n^{\circ} \text{ of isolated cells} > 20\mu\text{m} + n^{\circ} \text{ of isolated cells} < 20\mu\text{m}} \times 100 \quad (6)$$

$$\text{Depletion (\%)} = \frac{n^{\circ} \text{ of cells in inlet} - n^{\circ} \text{ of isolated cells}}{n^{\circ} \text{ of cells in inlet}} \quad (7)$$

2.10. Cell viability

The viability of isolated cells from devices two inlets/two outlets and two inlets/four outlets was assessed. Isolated cells from the outlets were collected, grouped, and centrifuged. Pellet was re-suspended in 500 μL of PBS and run into a third microfluidic platform designed and optimized for size-based isolation and enrichment of cancer cells at 10 $\mu\text{L}/\text{min}$ (87). After cell entrapment into the posts, Calcein-AM solution (12.5 $\mu\text{g}/\text{mL}$, Sigma) was injected into the

Microfluidic –based isolation of rare-tumor associated cells in prostate cancer

microfluidic device at 10 $\mu\text{L}/\text{min}$. In live cells, the non-fluorescent Calcein-AM is converted to a green fluorescent Calcein-AM after acetoxymethyl ester hydrolysis by intracellular esterases, so only viable cells will be fluorescent. After incubation of 30 minutes, washing with PBS was performed by injecting 500 μL PBS into the device at the same flow. Live cells were evaluated microscopically under a fluorescence microscope (Nikon Eclipse Ti). Figure 15 illustrates a schematic representation of this viability assay.

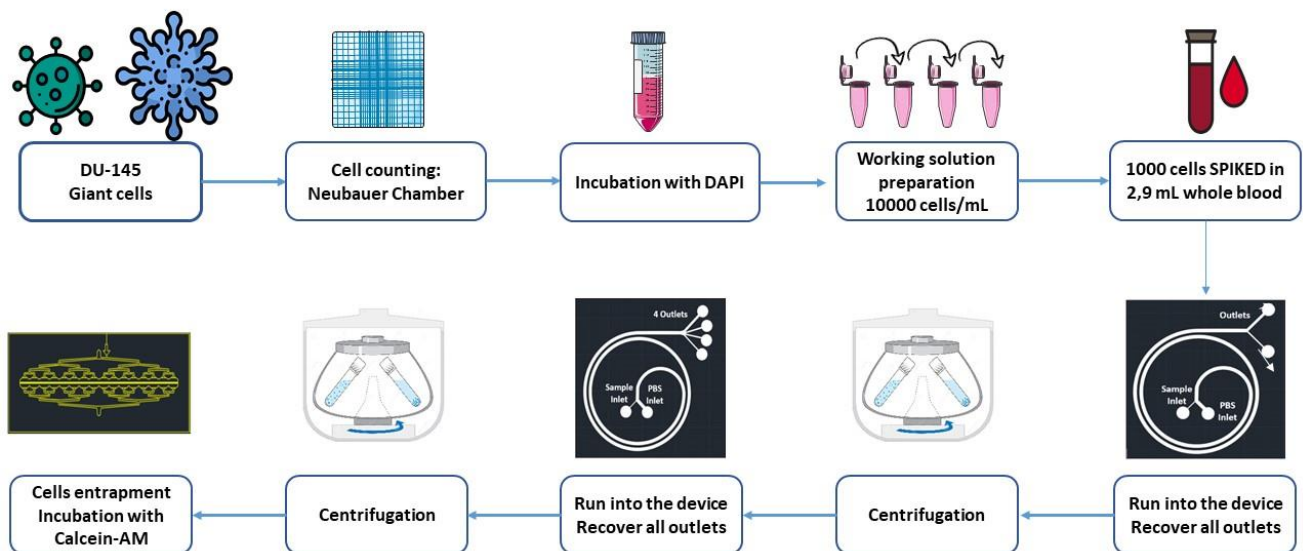


Figure 15- Schematic representation of the viability assays: 1000 DU-145 and Giant cells pre-stained with DAPI were spiked into PBS and run into the device with two inlets and two outlets with the flow rates of sample/buffer at 100/1000 $\mu\text{L}/\text{min}$. Then the recovered outlets (outlet 1 and 2) were centrifuged, reduced to 500 μL , and run into the device with two inlets and four outlets with the flow rates of sample/buffer at 100/1000 $\mu\text{L}/\text{min}$. Once again, all four outlets were recovered together, centrifuged, and run into a third microfluidic platform. Then the cells were counted under fluorescence microscope.

2.11. Statistical Analysis

Statistical analysis was performed using GraphPad Prism, version 8 (GraphPad Softwares, USA), and the applied test was Turkey's test. Data are presented as mean \pm standard error, with 95% of confidence. * $p < 0.01$, ** $p < 0.005$ and **** $p < 0.0001$.

3. RESULTS AND DISCUSSION

3.1. *In vitro* generation of giant cells

In order to perform optimization experiments for efficient microfluidic-based isolation of rare blood cells (CTCs and CAMLs) from PCa patients, we started by generating *in vitro* giant cells able to mimic the morphology features of CAMLs. These giant cells are obtained from human monocytes isolated from peripheral human blood and cultured under an appropriate medium supplemented with cytokines to induce the differentiation into mature macrophages (monocytes maturation) (88, 89). Giant cells have been reported to exhibit random arrangements of nuclei and widely variable cytoplasmic forms (circular or oval). These cells are remarkably large and able to join to form giant cell syncytia, which measure up to 1 mm in diameter (90).

Thus, human monocytes were isolated from healthy human whole blood and subjected to the following treatments to promote the generation of giant cells: IL-4 + IL-3 (10ng/mL each); IL-4 + GM-CSF (10ng/mL and 5ng/mL, respectively); IFN- γ + IL-3 (100U/mL and 10ng/mL, respectively); IFN- γ + GM-CSF (100U/mL and 5ng/mL, respectively); hM-CSF (50ng/mL), and hM-CS + IFN- γ + IL-3 (50ng/mL, 100U/mL and 10ng/mL, respectively). Every two days, the culture medium was replaced with a fresh one, and cell viability, growth, and morphology were daily assessed under the microscope. After ten days of treatment with cytokines, morphology and cell size (area) of adhered and suspended cells were evaluated (Figures 16 and 17, respectively). According to the literature, IL-4 is a potent human blood monocyte-derived macrophage fusion factor in the absence of other cytokines (90-92). IFN- γ is essential to suppress monocytes' maturation, promoting the clumping with no apparent fusion (92, 93). However, treatment of monocytes with only IL-4 or IFN- γ did not result in the formation of giant cells (Figure 16 (A)), possibly due to monocytes' deficient adhesion to the culture plastic surface. Other cytokines have been reported to be used in combination with IL-4 or IFN- γ to promote monocytes/macrophage adhesion and accelerate the acquisition of macrophage morphology (90, 92, 94). As showed in Figure 16 (A), treatments with IL-4 + IL-3 and IL-4 + GM-SCF generated giant cells with irregularly shaped morphology, like spindle, oblong and amorphous shapes, with only one nucleus. No major differences were observed in giant cell size when treated with IL-4 + IL-3 or IL-4 + GM-CSF (Figure 16 (B)). In contrast,

Microfluidic –based isolation of rare-tumor associated cells in prostate cancer

treatment of monocytes with IFN- γ + IL-3 and IFN- γ + GM-CSF resulted in giant cells with circular or ovoid shape, with one or more nuclei, often arranged in a characteristic circular or semi-circular “horseshoe” pattern (Figure 16 (A)). The polynucleated cells were observed once giant cells can exhibit phagocytic activity (95). Similar morphological features of giant cells under these specific cytokines treatments were reported by McNally and Anderson, 2011 (94). Treatment of monocytes with IFN- γ + GM-CSF resulted in a significant increase in giant cell size (Figure 16 (B)). Actually, GM-CSF has been reported to promote monocyte adhesion and macrophage development (90).

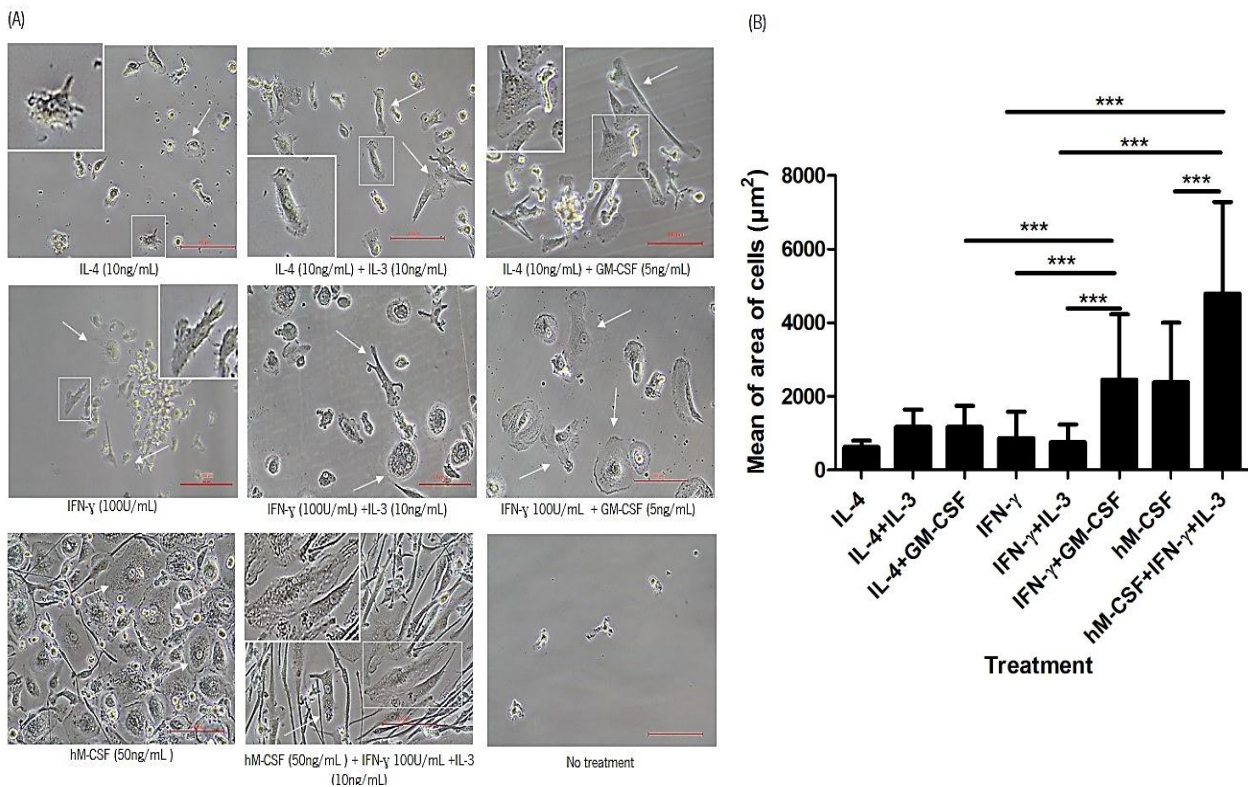


Figure 16- In vitro generation of giant cells. (A) Phase contrast images of giant cells after 10 days of treatment with cytokines. Scale bar 100 μm (B) Mean of area of adhered cells after 10 days of treatment with cytokines. Results are described as Mean +SD. * $p < 0.01$, ** $p < 0.005$ and *** $p < 0.0001$.

To promote cell adhesion, the monocytes were cultured with hM-CSF at the day of isolation and supplemented with IFN- γ + IL-3 at day 5. In fact, hM-CSF has been administrated by others (96) on the day of isolation because it is a cytokine with the potential to regulate the adhesion, proliferation, differentiation, and survival of monocytes (97, 98). As shown in Figure 16, treatment with hM-CSF and hM-CSF + IFN- γ + IL-3 resulted in giant cells with round and spindle-shaped. Most of the giant cells exhibit a large and round nucleus (Figure 16 (A)),

Microfluidic –based isolation of rare-tumor associated cells in prostate cancer

and a significant increase in cell size, when compared with other conditions, except for IFN- γ + GM-CSF that exhibit similar cell size (Figure 16 (B)).

Since the purpose of the *in vitro* generation of giant cells is to run them into the microfluidic devices and isolate them efficiently according to their size, their morphology and area were also evaluated after detachment at the end of the treatment. As expected, cells display a round morphology after detachment (Figure 17 (A)) and a decreased cell size when compared with adhered cells (Figure 16 (B) and 17 (B)). However, increased size of giant cells was observed in suspended cells after treatment with IFN- γ + IL-3, IFN- γ + GM-CSF, hM-CSF, and hM-CSF + IFN- γ + IL-3 (Figure 17 B). To note that a heterogeneous cell population regarding their size is verified at the end of treatment in all conditions, which result in a significant standard deviation (Figures 16 (B) and 17 (B)).

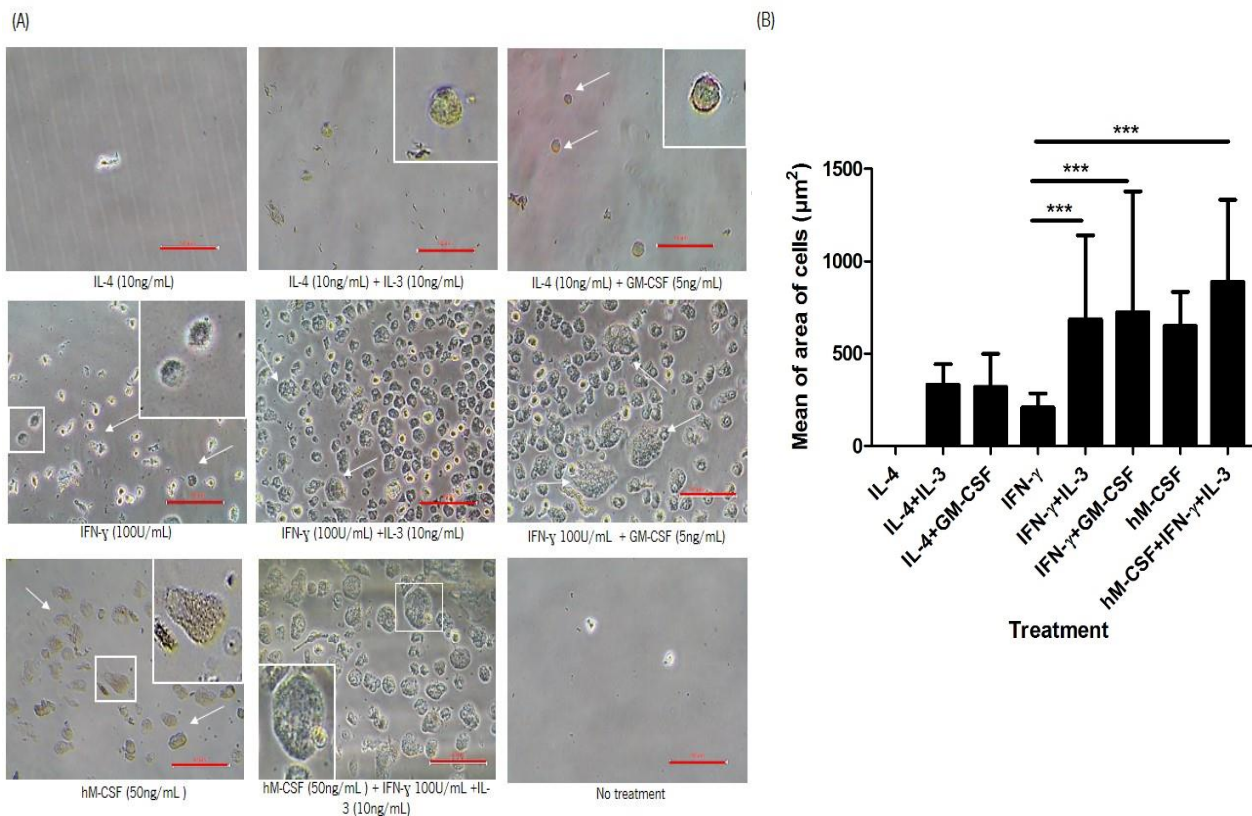


Figure 17- Suspended giant cells in the end of treatment with cytokines (A). Phase contrast images of giant cells after detachment from the plastic culture flask. Scale bar 100 μm (B) mean of area of suspended cells in function to the treatment that was applied. Results are described as Mean +SD of 1 independent experiments. * $p < 0.01$, ** $p < 0.005$ and *** $p < 0.0001$.

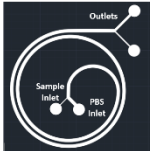
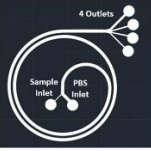
Taken together, these results suggest that treatment of monocytes with hM-CSF + IFN- γ + IL-3 induce an efficient monocytes fusion and thus bigger giant cells and suitable for optimization experiments with microfluidic devices (section 3.2).

3.2. Devices characterization and working principle

The primary design factor of a working spiral cell sorter is the need of having a correct channel depth that allows the inertial focusing of only large target cells near the inner wall while leaving the rest of the smaller untargeted cells dispersed and following the streamline away from the inner wall (86). From earlier reports, it was found that for particle separation based on the principle of DFF, the dimension of the channel need not be very small, which helps to fabricate such channel without using any sophisticated techniques (85).

After master moulds fabrication, measurements were performed, and PDMS replicas of the devices were obtained. Table 1 summarises the projected and real dimensions of specific regions of the microfluidic devices in the AutoCAD design and patterned wafer, respectively. Accurate depth is an important criterion to achieve to maximize the high efficiency of the devices. The correct depth of 170 μm was achieved in both devices. As it is possible to observe in Table 1, there is no significant difference between the dimensions projected and the real dimensions.

Table 1- Comparison between the dimensions projected in the CAD draw of the spiral devices and the pattern wafer width measurements, with an optical microscope and lent of 5x and 10x.

		Dimensions projected in the AutoCAD design (μm)	Pattern wafer width measurements (μm)
	Sample inlet	75	74.8
	Buffer inlet	500	500
	Channel width	500	499
	Outer outlet	350	351
	Inner outlet	150	149.5
	Depth	170	169.8
	Sample inlet	75	74.5
	Buffer inlet	500	499.2
	Channel width	500	499
	Channel expansion	890	850*
	Outer outlet	350	350
	Second outer outlet	210	209
	Third outer outlet	180	179
	Inner outlet	150	149.8
	Depth	170	170.2

Microfluidic –based isolation of rare-tumor associated cells in prostate cancer

The spiral microchannels have two inlets to accommodate the sample and buffer inflow at different flow rates and improve the separation of the target cells. To verify if the devices are focusing the desired cells to the correct outlet, a simple and fast test with a sample of polymethylmethacrylate (PMMA) microparticles suspended in dextran 40 (Dx 40) was performed. Thus, a suspension of PMMA microparticles ($\rho_{\text{PMMA}} = 1200 \text{ kg/m}^3$) in the range of 6 to 60 μm (6, 10, 20, 60) of diameter, suspended in Dx 40 at 10% (w/v) was prepared. The microparticles concentration was 2% (w/v) for the diameter of 6, 10 and 20 μm and 1% (w/v) for the 60 μm .

As we can see in Figure 18, the larger microparticles' focus was achieved through the inner wall. At the same time, smaller particles recirculate back to the external wall. Thus, it is possible to affirm that the device's design is performing a dean flow-focusing as was expected. By adding the bifurcation and the four outlets to the spiral device, the particles/cells will be subsequently separated into two or four groups based on their size, respectively. The significant advantage of the device with four outlets is the possibility to separate cells in different populations.

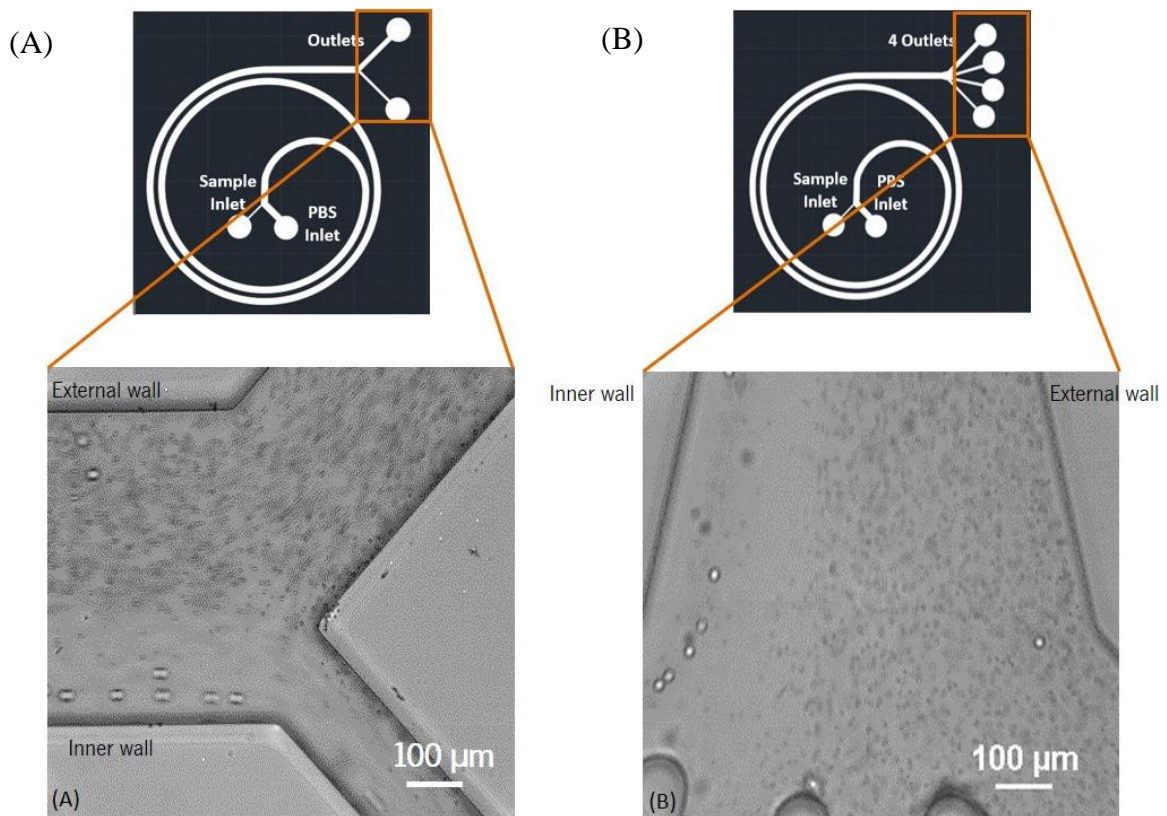


Figure 18- Working principle of the microfluidic system: larger target microparticles achieve full focusing on inner wall while non-target particles achieve the full focusing in the external wall (A) device with 2 inlets and 2 outlets. Scale bar 100 μm ; (B) device with 2 inlets and 4 outlets. Scale bar 100 μm .

Selection of such type of spiral geometry is based on the earlier reported works (84, 99-102) once cells may migrate across streamlines and be ordered in equilibrium positions based on their size, leading to label-free cell separation, purification, and enrichment in a microfluidic device (85, 103). Like other hydrodynamics-based devices (104-106), this spiral microfluidic system designed to isolate CTCs and CAMLs does not rely on antibodies or biological markers for labelling and isolate cells of interest (107). On the other hand, according to Bhagat et al., 2008, there is an inherent limitation of this passive microfluidic device design. The same device can only separate any particle/cell above and below a threshold size value, as long as the threshold particle size remains constant. For separations, where a change in the threshold size is needed, new devices must be designed and fabricated (100). Another limitation of this design is that in the spiral chip's operation, sheath fluid is used to influence particle focusing, which creates a larger collection volume that requires additional steps in order to isolated cells (86). However, the major advantage of these geometries is that these devices allow separating particles and/or cells with different sizes simultaneously. In particular, for this work, it was decided to perform the first step of isolation for cells over 20 μm , once the CTC and CAMLs have dimensions higher than that size (as previously demonstrated in section 2.4), and in this way, isolated them from the other components of blood cells. With the device with 2 inlets / 4 outlets, a refinement of the isolation is performed, removing the remaining contamination of RBCs and isolating the CTCs and CAMLs individually. Besides that, some researchers developed a spiral micro-channel of comparatively larger dimensions for the separation of polymeric microparticles based on their dimension and showed that this design could also be applied to large-sized biological cells or CTCs (99). With these results, they showed the versatility of this type of device.

3.3. Devices flow rates optimization

After design and fabrication, flow rates of sample and buffer were optimized to maximize the further microfluidic-based isolation efficiency of target cells (next section). In microfluidic systems, the flow rates ratio can influence separation performance (86, 106, 108, 109). Since CTCs and CAMLs are rare in the blood stream (i.e., ~3 and ~5 cells per 7.5 mL of blood, respectively), it is extremely crucial to isolate a maximum number of target cells with a low background of WBCs and RBCs (42, 86, 108). To determine the proper flow rates for sample and buffer, a cell suspension of DU-145 and giant cells were added to PBS and injected into the devices at flow rates of 100 or 200 $\mu\text{L}/\text{min}$. The optimal flow rate ratio between sample/buffer proposed by Hou et al., 2013 is 1:9, for a close design of spiral devices (33, 86). Thus, the flow rates tested for the buffer (PBS) injection through the device with two inlets and two outlets were 600, 800, 1000 and 1200 $\mu\text{L}/\text{min}$. Buffer flow rates of 500, 600, 800, 1000 and 1200 $\mu\text{L}/\text{min}$ were tested in the device with two inlets and four outlets. After running cell suspension into the devices, cell recovery was evaluated by the ratio between the number of cells in the interest outlets over the total number of cells recovered in all outlets. This way of measuring efficiency has been used by several authors because it is faster and equally efficient (110). To note that DU-145 cells display an average cell size of $15 \pm 2.8 \mu\text{m}$ (Figure 19), which indicates that our microfluidic systems will not efficiently recover them.

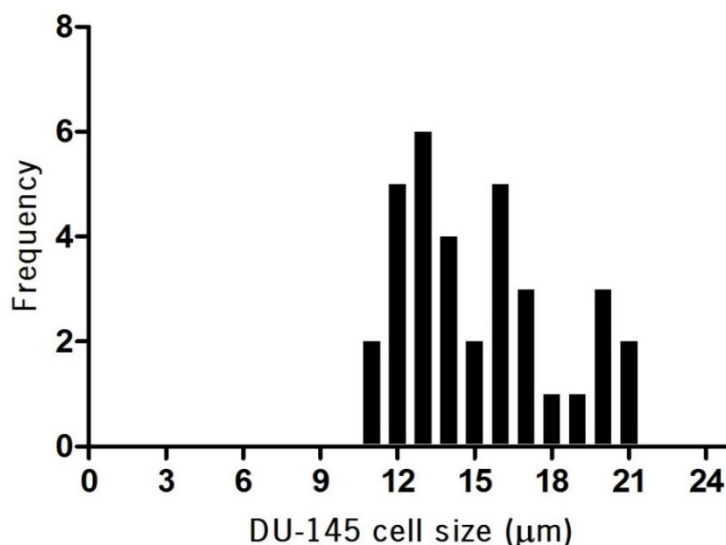


Figure 19- Size distribution of DU-45 cells. Key statistical parameters of DU-145 cells (diameter): min 11.008 μm ; max 21.075 μm ; mean 15.1974 μm ; SD: 2.954 μm .

However, giant cells that exhibit a larger size (Figure 20), $28.412 \pm 9.263 \mu\text{m}$ than the established size threshold, will be recovered by both devices.

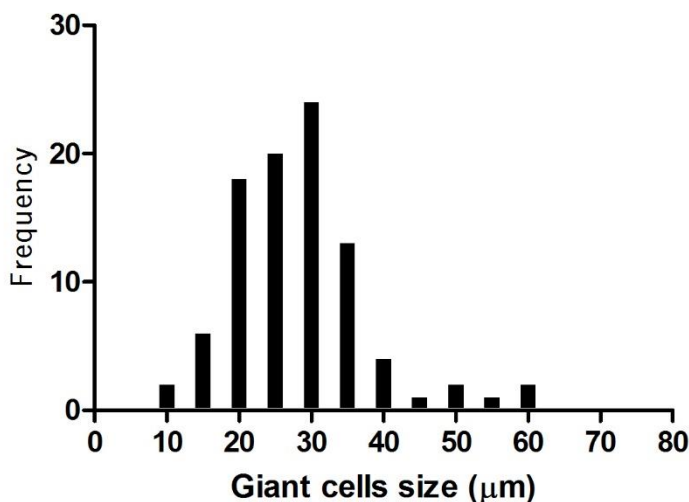


Figure 20- Size distribution giant cells Key statistical parameters of giant cells (diameter): min 12.172 μm ; max 61.3685 μm ; mean 28.412 μm ; SD: 9.263 μm .

For the device with two outlets, with the sample running at 100 $\mu\text{L}/\text{min}$ and by increasing the buffer flow rate, the best results were obtained for the combination of 100/1000 $\mu\text{L}/\text{min}$, with a recovery efficiency of the giants' cells ($> 20 \mu\text{m}$) of 87.17% (Figure 21 (A)) and DU-145 cells ($< 20 \mu\text{m}$) of 14.97% (Figure 21 (B)). Note that the cancer cell line has a mean diameter of 15.2 μm , thus these cells will be discarded through outlet 1 since we pretend to recover cells over 20 μm . By increasing the buffer flow rate for 1200 μL , a significant reduction ($P < 0.0001$) of the recovery of cells over 20 μm is obtained (Figure 21 (A)). In this case, a pulsatile flow inside the device was observed (visible at the naked eye). That phenomena cause instabilities in the correct focusing of the cells, leading to an increase in the recovery of cells bellow 20 μm (DU-145) and a decrease in the capture of cells $> 20 \mu\text{m}$.

Increasing the sample flow rate to 200 $\mu\text{L}/\text{min}$ and working with the buffer at 600, 800 or 1000 $\mu\text{L}/\text{min}$, the recovery efficiency of cells $< 20 \mu\text{m}$ do not present significant differences (Figure 21 (B)); however, an increase in the recovery of cells over than 20 μm is observed (Figure 21 (A)). Since it is pretended a maximum recovery of target cells (giant cells), with minimum contamination of other cells, the flow rate with better results for the spiral device with 2 outlets is 100/1000 $\mu\text{L}/\text{min}$, close to the one proposed by Hou et al., 2013 (111).

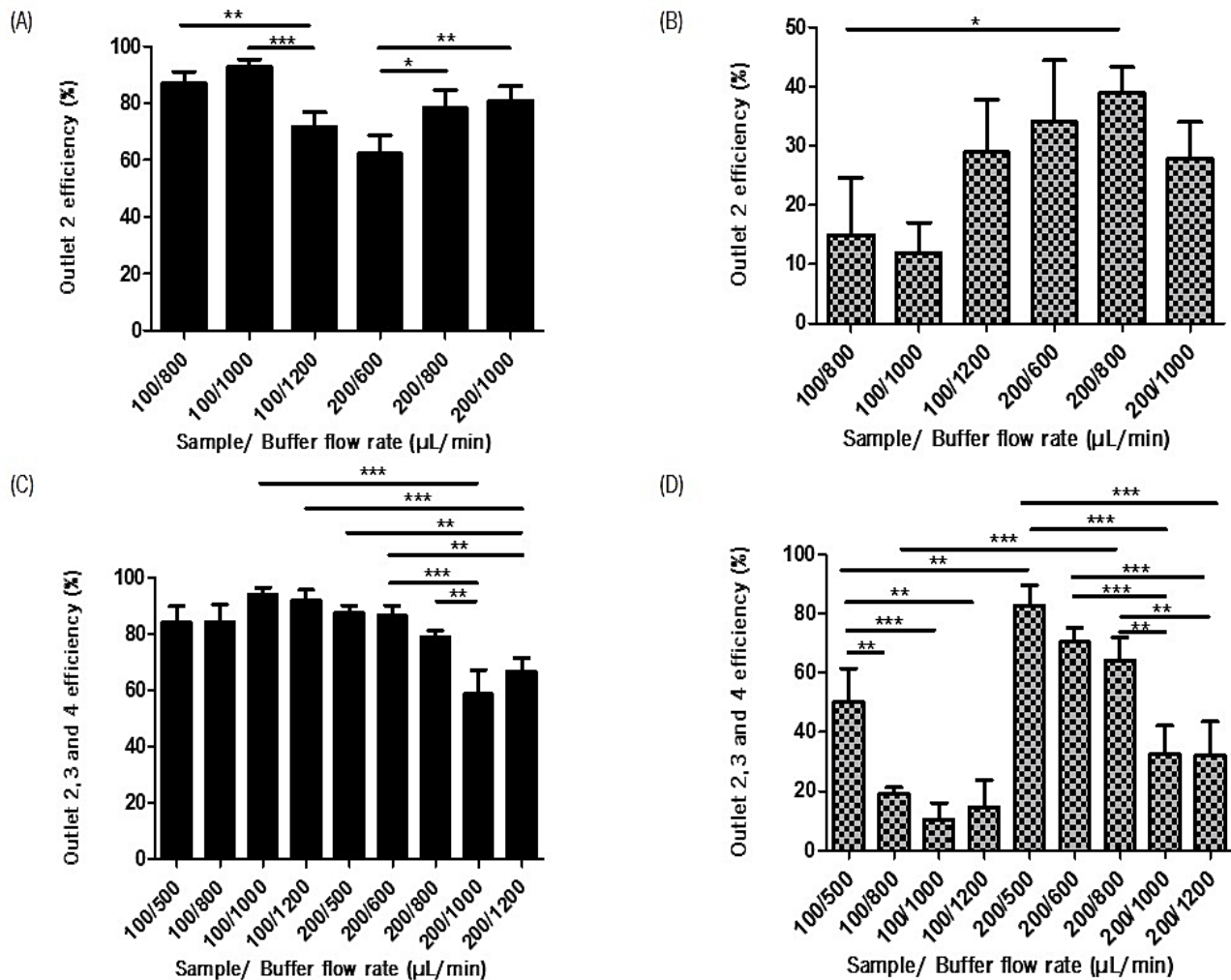


Figure 21- Average isolation efficiency obtained for each device of giant cells and Du-145 of three different experiments for runs at different flow rates of sample/buffer ratio. (A) Giant cells suspended into PBS and run in the device with 2 inlets/2 outlets; (B) DU-145 suspended into PBS and run in the Device with 2 inlets/2 outlets; (C) Giant cells suspended into PBS and run in the Device with 2 inlets/4 outlets; (D) DU-145 suspended into PBS and run in the Device with 2 inlets/4 outlets. Results are described as Mean +SD of 3 independent experiments. * $p < 0.01$, ** $p < 0.005$ and *** $p < 0.0001$.

For the device with 4 outlets, several ratios between the buffer and sample flow rates were tested (Figure 21 (C, D)). Again, the increase of the sample flow rate for 200 μL decreases the recovery of cells with dimensions over 20 μm (Figure 21 (C)), generating possible contamination of the outlets. Also, the recovery of the Du-145 is higher, as is possible to observe by the outlets' efficiency in Figure 21 (D). For the sample flow rate at 100 μL/min and increasing the buffer flow rate, better results were obtained. Regarding the ratios of 100/800, 100/1000, and 100/1200 μL/min, the best results were obtained since higher outlets efficiency. Consequently, lower recoveries were obtained, i.e., a high amount of cells > 20 μm is recovered, and lower quantities of cells < 20 are captured. In particular, with the flow rate

of 100/1000 $\mu\text{L}/\text{min}$, a lower quantity of cells $< 20 \mu\text{m}$ is obtained. Notably, the best performance of each device is obtained by using the flow rate ratio of 100/1000 $\mu\text{L}/\text{min}$, respectively sample/buffer, with 92.80% for cells $> 20 \mu\text{m}$ and 11.90% for cells $< 20 \mu\text{m}$ for the device with two inlets and two outlets and 93.79% for the larger cells and 10.50% for cells $< 20 \mu\text{m}$ for the device with 4 outlets.

As Pamme et al., 2007 discuss in a review, continuous flow separation techniques are becoming popular on the microscale due to their ability to achieve high sample throughputs (99, 112). Warkiani and colleagues developed a device that showed spiked cells' recoveries around 85% cancer cell lines (MCF-7, T24, and MDA-MB-231) for lysed blood samples when was injected at 1700 $\mu\text{L}/\text{min}$. Even though this device presents a similar recovery rate and can operate at a higher sample flow rate, the RBCs lysis leads to a loss of cells during the entire process compared to our microfluidic devices. Besides that Hou et al., 2016 used a single spiral microchannel with two inlet and four outlets to isolate and purify neutrophils from small blood volumes (fingerpick $\sim 130 \mu\text{L}$) with the larger neutrophils and monocytes being sorted ($> 80\%$) into the outlet and the majority of the smaller lymphocytes ($\sim 95\%$) being separated into outlet 3 (106).

Thus, both devices proposed in this work, to obtain their higher isolation efficiency, the flow rates of 100/1000 $\mu\text{L}/\text{min}$, respectively sample/buffer, need to be applied.

3.4. DU-145 and Giant cells microfluidic-based efficiency

To test the performance of the spiral biochip system for the isolation of CTCs and CAMLs and determine their recovery rates, increasing number, 50,100,1000 and 2000 of DU-145 and giant cells (pre-labelled with DAPI and Calcein-AM, respectively) were spiked in diluted whole blood from healthy individuals and processed through the microfluidic system at flow rates of 100/1000 $\mu\text{L}/\text{min}$. Note that the microfluidic system is composed of both devices, i.e., the spiked sample is processed through the microfluidic device with two inlets and two outlets. Thus outlet 2 is recovered, centrifuged at 1200 rpm for 5 minutes, and pellet reduced to 1000 μL . This later cell suspension is then processed through the microfluidic device with two inlets/ four outlets. After isolation steps, each outlet was recovered and counted by observation using a fluorescence microscope.

Microfluidic –based isolation of rare-tumor associated cells in prostate cancer

As previously described, the average size of DU-145 cells was $15.19 \pm 2.83 \mu\text{m}$ (Figure 19), and the size threshold taken into consideration in the designing process has been established as $20 \mu\text{m}$ (see section 3.2). For those reasons, DU-145 cells were preferentially depleted in outlet 1 of device two inlets/ two outlets (Figure 22 (A)). Thus the depletion of DU-145 cells can be determined by using equation 7 described in section 2.9.

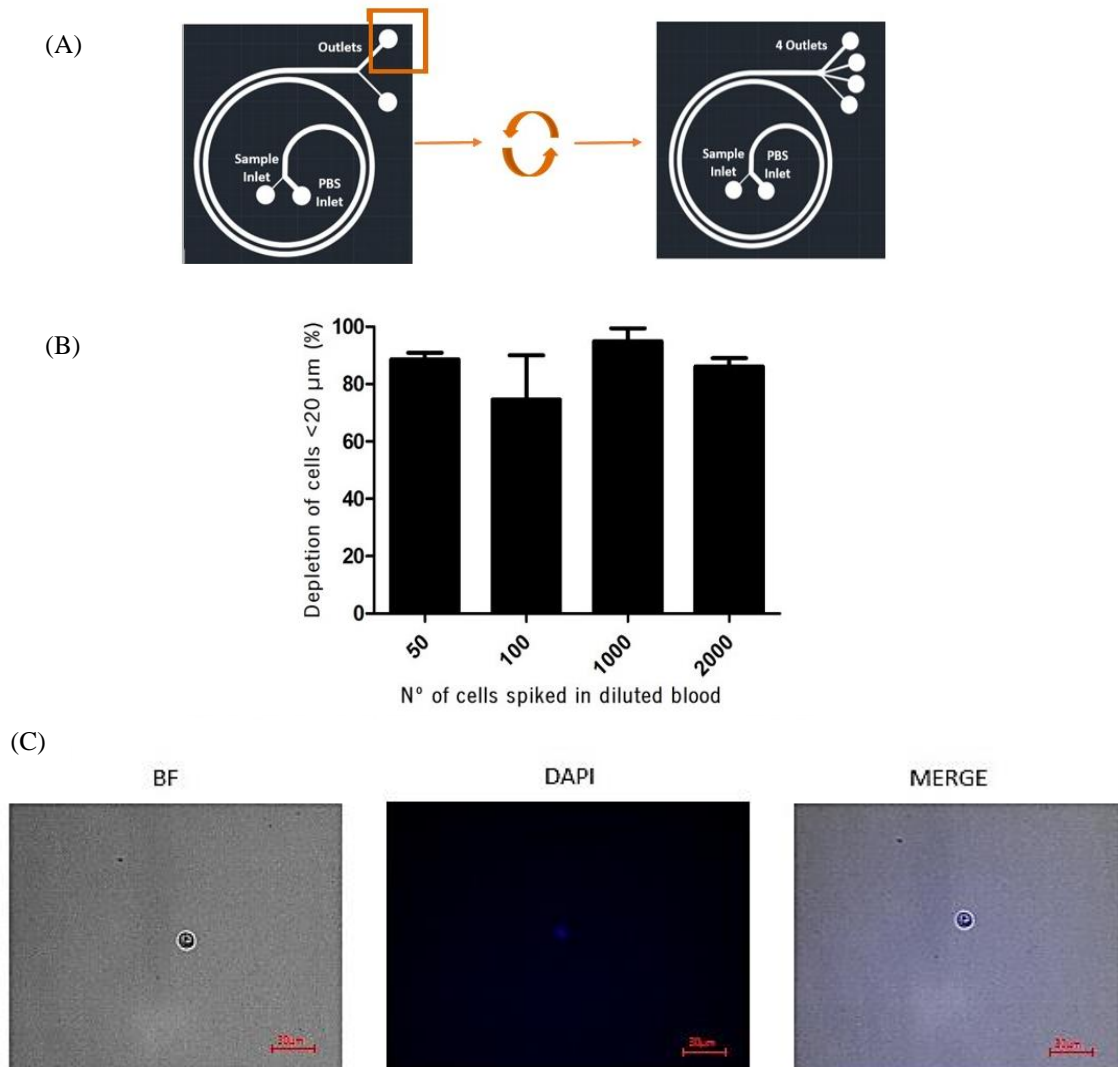


Figure 22- Cells < $20 \mu\text{m}$ depletion in function to the number of cells spiked in diluted blood and Cells < $20 \mu\text{m}$ isolated by the device (A) Schematic identification of the target outlets; (B) Average depletion of cells < $20 \mu\text{m}$ per outlet of three different experiments. 50, 100, 1000 and 2000 spiked cells in the diluted blood were run into the device with 2 inlets and 2 outlets with the flow rates of sample/buffer at $100/1000 \mu\text{L}/\text{min}$, then the recovered outlet 2 was centrifuged, reduced to $1000 \mu\text{L}$ and run into the device with 2 inlets and 4 outlets with the flow rates of sample/buffer at $100/1000 \mu\text{L}/\text{min}$. Results are described as Mean \pm SD of 3 independent experiments. (C) Cells < $20 \mu\text{m}$ pre-stained with DAPI recovered. Images obtained with the objective lens of 20x. Scale bar $30 \mu\text{m}$. * $p < 0.01$, ** $p < 0.005$ and **** $p < 0.0001$.

The average percentage of DU-145 cells depleted through the system, i.e., depleted through outlet 1 of the device with two inlets/ two outlets, does not represent significant

differences regarding the cells spiked ($P=0.0839$) (Figure 22 (B)); thus it is possible to say that a high depletion of cells $< 20 \mu\text{m}$ is obtained. One of the limitations of using our device for CTC isolation is that performance in terms of sensitivity and recovery will be compromised when a significant size overlap of target and non-target cells exists. CTCs have a wide distribution of size depended on cancer type. (86). Figure 22 (C) shows one example of isolated DU-145 cells analysed by bright field and fluorescence microscopy.

To address the recovery of cells over $20 \mu\text{m}$, 50, 100, 1000, and 2000 giant cells pre-labelled with Calcein-AM were spiked in diluted blood and processed through the microfluidic system. Since the majority of cells analysed have a diameter more significant than the threshold of the system ($20 \mu\text{m}$), they will be isolated by the outlets of the device with two inlets/four outlets (Figure 23 (A)). Therefore, the efficiency in recover the cells was determined using Equation 5, described in section 2.9.

According to Figure 23 (B), the average percentage of cells $> 20 \mu\text{m}$ recover through the system remains around 76% when are low spiked number of cells (50, 100) and 10% when are spiked 1000 or 2000 cells. This significant decrease ($P<0.0001$) could be due to the fact of giant cells presenting a higher length and an irregular shape that allows the aggregation of cells and increase the cell-to-cell interactions, leading to entrapment in the critic zones of the device geometry and changes in the focusing equilibrium position of cells. It can also occur in the sedimentation of cells due to the depth of the channels. Despite the decrease in efficiency with the increasing number of spiked cells and regarding the isolated cells, most of them are being isolated mainly through outlets 2 and 3 (Figure 23 (C)). Theoretically, it was expected that CAMLs would be mostly separated in outlet 3 with some going to outlet 4 due to their size dimensions, i.e., cells over $20 \mu\text{m}$ will focus on the inner wall. However, given the heterogeneity of cells generated *in vitro* regarding the size (Figure 20), it was impossible to control the diameter of selected cells. The sample of the giant cells has cells under $20 \mu\text{m}$, which ended up influencing the respective recovery rate. Figure 23 (D) shows one example of isolated cells analysed by bright field and fluorescence microscopy.

Microfluidic –based isolation of rare-tumor associated cells in prostate cancer

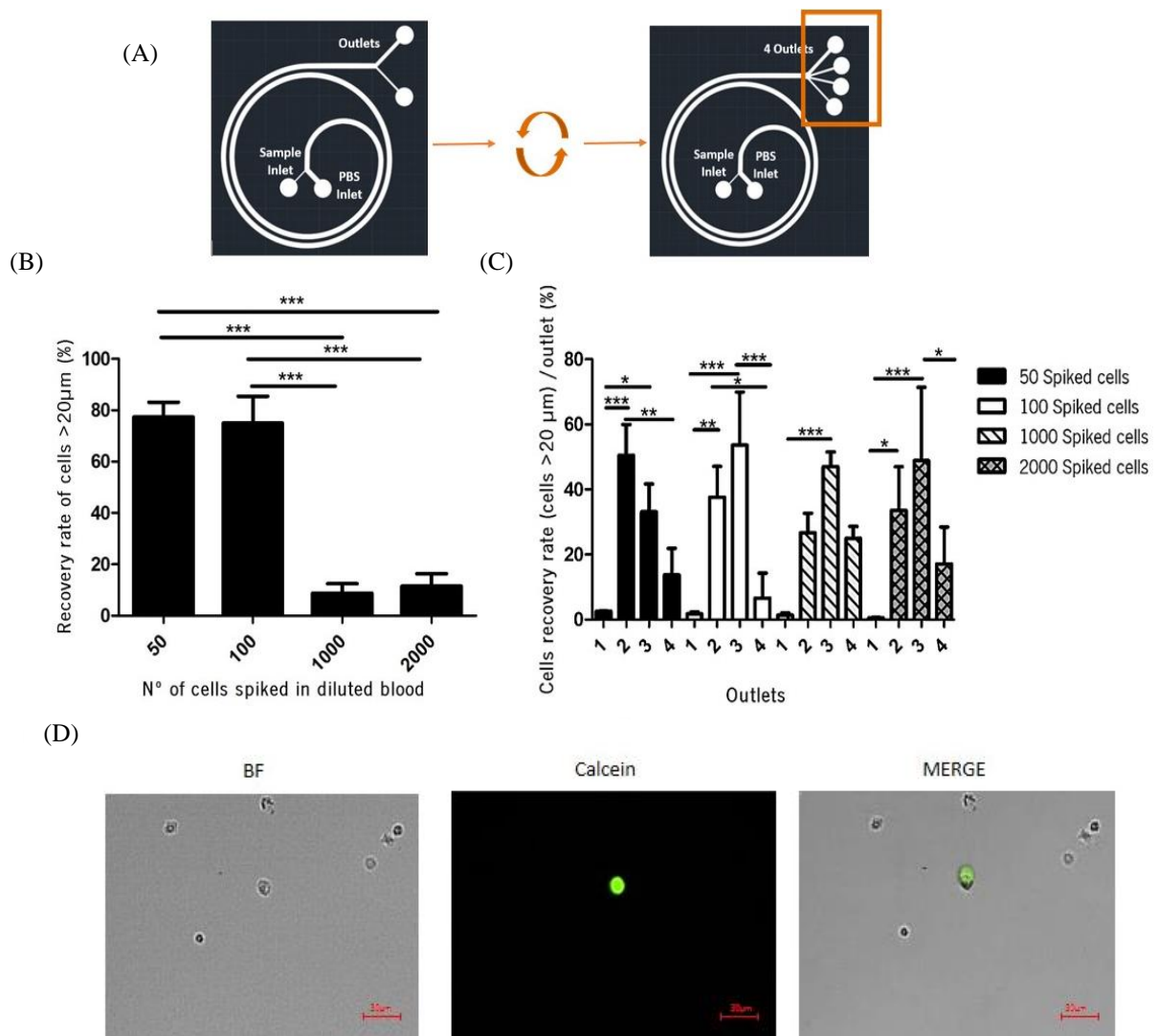


Figure 23- Cells > 20 μm recovery in function to the number of cells spiked in diluted blood (A) Schematic identification of the isolation microfluidic system and target outlets; (B) Average recovery rate of three different experiments. 50, 100, 1000 and 2000 spiked cells in the diluted blood were run into the device with 2 inlets and 2 outlets with the flow rates of sample/buffer at 100/1000 μL/min, then the recovered outlet 2 was centrifuged, reduced to 1000 μL and run into the device with 2 inlets and 4 outlets with the flow rates of sample/buffer at 100/1000 μL/min. Error bars represent standard deviation; Results are described as Mean +SD of 3 independent experiments (C) Average recovery rate of cells > 20 μm per outlet in function of the isolated cells for three different experiments. 50, 100, 1000 and 2000 spiked cells in the diluted blood were run into the device with 2 inlets and 2 outlets with the flow rates of sample/buffer at 100/1000 μL/min, then the recovered outlet 2 was centrifuged, reduced to 1000 μL, and run into the device with 2 inlets and 4 outlets with the flow rates of sample/buffer at 100/1000 μL/min. Error bars represent standard deviation. Results are described as Mean +SD of 3 independent experiments (D) Cells > 20 μm pre-stained with Calcein-AM recovered. Images obtained with the objective lens of 20x. Scale bar 30 μm. *p<0.01, **p<0.005 and ****p<0.0001.

Spiking experiments of both cells at the same time were performed to address the cells $> 20 \mu\text{m}$ recovery rate and the cells $< 20 \mu\text{m}$ depletion. With the combination of both populations in the same sample, we can better represent the future pathological sample. Both cells flow in the microfluidic system simultaneously with 50, 100, 1000, and 2000 cells of each, pre-labelled with Calcein-AM and DAPI, respectively, for cells over $> 20 \mu\text{m}$ and cells size lower $20 \mu\text{m}$, spiked in of diluted blood. The isolation efficiency and the depletion of cells were determined using the equations presented before in section 2.9.

Results (Figure 24 (B)) show that, for spiking experiments, the combination of both cells population influence the cells isolation. There was a decrease in recovery rates regarding the tests performed with the cells spiked separately (Figure 22 (B) and Figure 23 (B)). This suggests that the combination of DU-145 and giant cells can be influencing the equilibrium positions of cells and thus affecting the respective depletion and recoveries. Figure 24 (C) shows an example of isolated cells analysed by bright field and fluorescence microscopy. Once again, low recovery rates for spiking high cell number and high recovery rates for low cell spiking levels are observed. Thus, the recovery rate for cells over $20 \mu\text{m}$ was 72.67, 83.33, 19.20, 12.8 % for 50, 100, 1000, and 2000 spiked cells. Regarding the cells $< 20 \mu\text{m}$, the depletion rate increases with the number of spiked cells, presenting values of 66, 76.67, 90, and 94%. Since we have two different populations of cells regarding the sizes, it was possible to evaluate the target cell's purity, i.e., cells $> 20 \mu\text{m}$. The results present the following values 70, 78, 66, and 69%. Given this result, this microfluidic system presents to be a good option for cell separation, and with sequential passages of the fluid their efficiency and outlet sample purity can be improved.

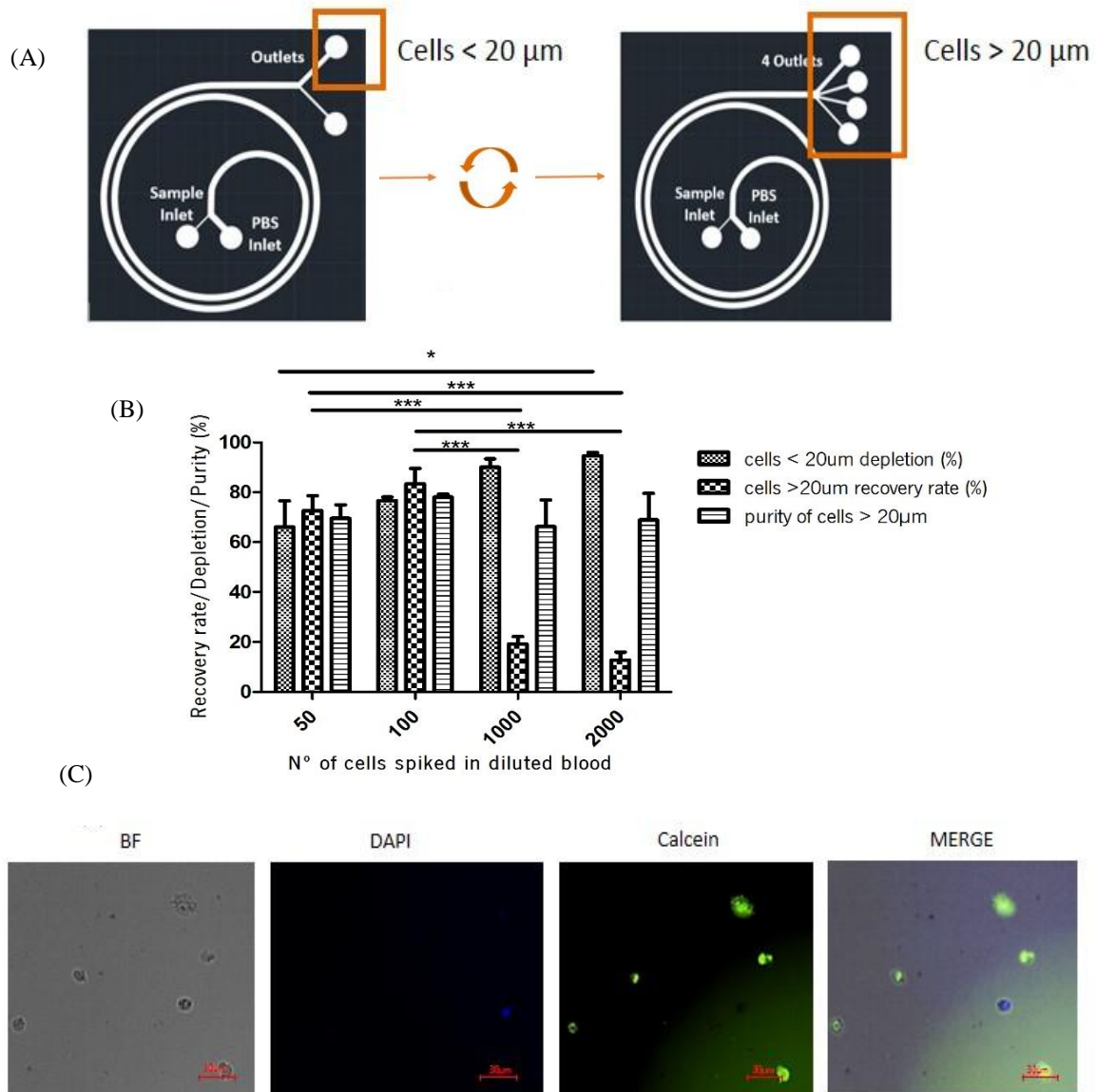


Figure 24- Cells $> 20 \mu\text{m}$ recovery rate and Cells $< 20 \mu\text{m}$ depletion efficiency in function to the number of cells spiked in diluted blood and $20 \mu\text{m} < \text{Cells} < 20 \mu\text{m}$ isolated by the device (A) schematic representation of the target cells outlets; (B) Average recovery rate and depletion efficiency of three different experiments. 50, 100, 1000 and 2000 spiked cells in the diluted blood were run into the device with 2 inlets and 2 outlets with the flow rates of sample/buffer at 100/1000 $\mu\text{L}/\text{min}$, then the recovered outlet 2 was centrifuged, reduced to 1000 μL , and run into the device with 2 inlets and 4 outlets with the flow rates of sample/buffer at 100/1000 $\mu\text{L}/\text{min}$. The depletion was measured using a ratio between the number of cells inserted in inlet less cells counted in outlets and cells inserted in inlet. Error bars represent standard deviation; Results are described as Mean \pm SD of 3 independent experiments (C) Cells $< 20 \mu\text{m}$ pre-stained with DAPI and Cells $> 20 \mu\text{m}$ pre-stained with Calcein-AM recovered. Images acquired for bright field BF, DAPI Calcein-AM and merge Images obtained with the objective lens of 20x. Scale bar 30 μm . * $p < 0.01$, ** $p < 0.005$ and **** $p < 0.0001$.

These spiral biochip system proposed have demonstrated their superiority over the only FDA-approved platform for CTCs enumeration, CellSearch™ (113, 114), since the last has the working principle based on immunomagnetic enrichment with fluorescent labelling (114-116), which is considered an issue once CTC presents heterogeneity and the expression of

EpCAM and CK vary among the different population (64, 65). The proposed system uses a passive hydrodynamic method for isolation, been only dependent on the size of cells, recovering the cells for further downstream applications. The CellSearch™ has also been applied by Adams et al., 2016 and Mu et al., 2017 for CAMLs isolation (117, 118). However, while CAMLs are easy to identify by their large size and multi nucleus, their expression of multiple heterogeneous markers has defined conventional characterization and have made study difficult using most isolation technologies (117). The proposed microfluidic system comes to overtake this issue and is comparable to the CellSieve™ where microfilters with 7 μm pores were used to isolate CAMLs and CTCs from 7.5 mL whole peripheral blood. CellSieve™ microfilters are size-exclusion membranes that efficiently isolate CAMLs and circulating tumor cells (CTCs) from whole blood, making it possible to study both cell types (117, 119). This system was used by Adams et al., 2016 where they identified at least one CTC in 72% of the patient sample and 28 CAMLs in 29 blood samples, while CellSearch™ identifies at least one CTC in 58% of samples.

Related to the purity of outlets in terms of having cells below 20 μm (DU-145) in the recover outlets samples, this parameter remains almost constant for all conditions tested once there are no significant differences regarding the number of cells spiked in diluted blood ($P = 0.752$). According to other research, it is necessary to consider the purity of each outlet sample in relation to the cellular composition of the original sample. It is known that significant differences in cellular populations lead to higher contamination of the outlets. Refer that in the results obtained for the experiments with both cells, the microfluidic system can separate the giant cells from the DU-145. However, the possible contaminations from other blood cells population, namely WBCs, as other authors reported is not quantified (86, 87, 106). That is an important consideration since an overlap in cell sizes can reduce the outlet fraction's purity (109).

3.5. Viability of isolated cells from microfluidic devices

To evaluate the viability of the isolated cells from a microfluidic system composed by the device with two inlets and two outlets and the device with two inlets and four outlets, 1000 cells (DU-145 representing cells $< 20 \mu\text{m}$; and giant cells representing cells $> 20 \mu\text{m}$) were pre-labelled with DAPI, isolated by the microfluidic system and subjected to a run into a third microfluidic platform to promote the capture of isolated cells and their visualization under a fluorescent microscope. This third microfluidic platform consists of five rows of posts, with increasingly narrower gap widths (50, 20, 15, 10, and $5 \mu\text{m}$) to separate cells according to their size and deformability (87). After, captured cells were stained with Calcein-AM, a cytoplasmic marker. In live cells, the non-fluorescent Calcein-AM is converted to a green fluorescent Calcein-AM after acetoxymethyl ester hydrolysis by intracellular esterases, so only viable cells will be fluorescent. As shown in Figure 25, some captured cells are viable (DAPI-positive and Calcein-AM-positive), and others are non-viable (DAPI-positive and Calcein-AM-negative).

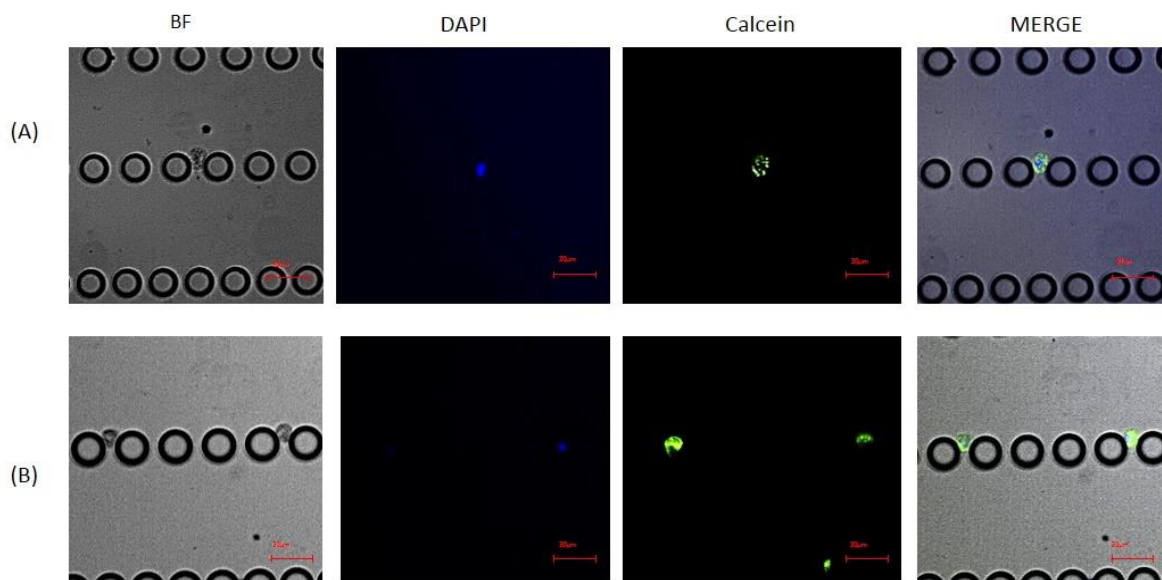


Figure 25- Cells viability assay. After running 1000 cells pre-stained into the microfluidic system at $10 \mu\text{L}/\text{min}$ the recovery sample was run into the device with 5 rows designed by the group. Calcein-AM cell viability assay was made to verify the viability of isolated cells. (A) Captured cells $< 20 \mu\text{m}$; (B) captured cells $> 20 \mu\text{m}$. Images obtained with the objective lens of 20x. Scale bar $30 \mu\text{m}$.

The some of the previously isolated cells from the microfluidic system composed of the two spiral devices is non-viable can be related to some damages into the cells due to the high flow rates used inducing high shear stress and internal pressure inside of the microchannels.

Microfluidic –based isolation of rare-tumor associated cells in prostate cancer

The cell viability experiment also demonstrated a low number of cells captured in the device with five rows of posts that did not correspond to the initial efficiency rates. To ascertain such loss, a control sample of DU-145 and giant cells (1000 each) were injected into the device with two inlets/ two outlets and was counted. Only 300 cells were counted. Various events can lead to the loss of a significant number of cells: pipetting and serial dilutions associated error, aggregation, and deposition of the cells in the depth of the channel, and intermediate centrifugation. During centrifugation, it is expectable that a 10% decrease in the number of cells occurs. As cell loss is greater than 10%, it is impossible to affirm that this procedure is the most responsible for the loss of cells. Thus, it is possible to affirm that the device is mostly losing the cells. At the end of the runs, after a microscope inspection, it was observed that the first device presents some damage in the walls, Figure 26. This can be one of the significant problems for isolation efficiency reduction.

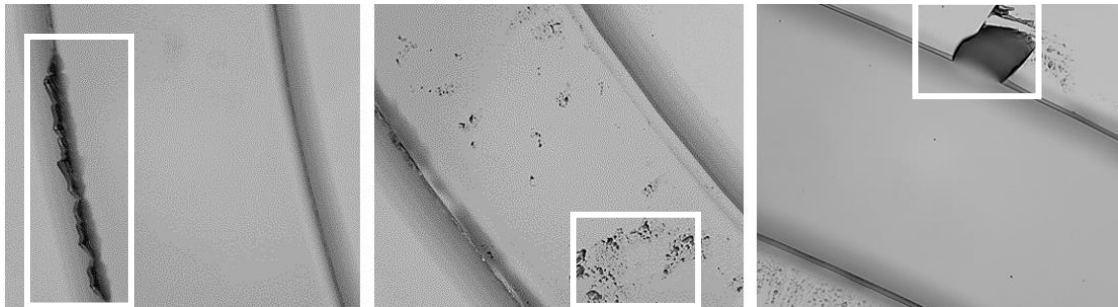


Figure 26- Microscope images of the device 2 inlets/2 outlets channels. As observer the walls have several damages.

However, other reports showed that the viability of the sorted cells in the microchannel remained above >90%, with most cells retaining their initial morphology. Tae et al. 2014 show that the viability of the sorted MCF-7 cells remained above >90% without incurring gross physical damage and Wong et al. 2011 show that the viability of the hMSCs sorted cells was similar to that of the unsorted (control) with more than 90% of the cells collected from each outlet excluding the dye; this suggests that hMSCs were sorted without incurring gross physical damage. After 14 days of culture, the morphology of the sorted hMSCs was similar to that of the unsorted (control) cells, further demonstrating the maintenance of cell viability post-sorting (120, 121). These reports reinforce the hypothesis that our microfluidics system can isolate cells with high efficiency and viability at the same time. It would be necessary to improve some parameters to, consequently, improve the results.

4. CONCLUSION AND FUTURE WORK

The main goal of cancer medicine is the establishment of personalized therapies. CTCs are an excellent alternative to primary tumor biopsies, as they carry similar genetic information. However, some researchers propose that CTCs are not sufficient to develop metastasis, showing that CAMLs interact with CTCs, hitting a role for CAMLs in cancer cell dissemination. Liquid biopsy, which is based on finding rare tumour-associated cells in a blood sample of cancer patients at various disease stages, is a promising prognostic marker for treatment efficacy and patient survival, indicating strong clinical relevance. However, these rare cells' characterisation has been delayed by the lack of reliable and sensitive methods to detect and enrich these cells. Despite the rapid advances in microfluidic technologies, there is no microfluidic approach capable of isolating CTCs and CAMLs individually with high throughput, high purity, and increased cell viability. In this work, we demonstrated the application of a novel microfluidic system for isolation CTCs and CAMLs using inertial microfluidic employing spiral microchannels.

The microdevice previously designed by the group was used to perform cancer cell isolation based on cell size. Despite the loss of cells during the isolation, this microfluidic system can retain cells of interest in a heterogeneous sample. Thus, the design of the devices needs to be optimized to avoid cell loss. For clinical sample analysis, improvement and optimization of the isolation process and decontamination of red blood cells were necessary, given its complexity and time consuming and further complicated outlet sample evaluation. Thus, the devices' direct combination could be studied instead of running samples in the two devices separately, with intermediate centrifugation. Also, the lysis of red blood cells before running the sample in the microfluidic device could be applied.

Further studies with a panel of distinct biomarkers need to be evaluated and validated for adequate phenotypic characterisation of DU-145 and cells generated *in vitro*. In future experiments, clinical samples from PCa patients will be performed in the optimized microfluidic device final prototype to collect CTCs and CAMLs independently for further phenotypic characterisation. Nevertheless, once this approach does not require initial cell surface biomarker selection, it is suitable for different cancers. The proposed design is versatile and can separate particulate mixtures over a wide dynamic range by moderate alterations of the channel design.

Microfluidic –based isolation of rare-tumor associated cells in prostate cancer

In conclusion, even though some issues need to be optimized, the proposed microfluidic device may provide a promising point-of-care application that contributes to a better understanding of the clinical significance of the separation of the cells and elucidate novel molecular targets for future therapeutic approaches.

REFERENCES

1. Wong MCS, Goggins WB, Wang HHX, Fung FDH, Leung C, Wong SYS, et al. Global Incidence and Mortality for Prostate Cancer: Analysis of Temporal Patterns and Trends in 36 Countries. *European Urology*. 2016;70(5):862-74.
2. Gann PH. Risk factors for prostate cancer. *Rev Urol*. 2002;4 Suppl 5(Suppl 5):S3-S10.
3. Hassanipour-Azgomi S, Mohammadian-Hafshejani A, Ghoncheh M, Towhidi F, Jamehshorani S, Salehiniya H. Incidence and mortality of prostate cancer and their relationship with the Human Development Index worldwide. *Prostate International*. 2016;4(3):118-24.
4. Malik SS, Batool R, Masood N, Yasmin A. Risk factors for prostate cancer: A multifactorial case-control study. *Current Problems in Cancer*. 2018;42(3):337-43.
5. Grönberg H. Prostate cancer epidemiology. *The Lancet*. 2003;361(9360):859-64.
6. Patel AR, Klein EA. Risk factors for prostate cancer. *Nature Clinical Practice Urology*. 2009;6(2):87-95.
7. Barron DA, Rowley DR. The reactive stroma microenvironment and prostate cancer progression. *Endocr Relat Cancer*. 2012;19(6):R187-R204.
8. Omabe M, Ezeani M. Infection, inflammation and prostate carcinogenesis. *Infection, Genetics and Evolution*. 2011;11(6):1195-8.
9. De Marzo AM, Platz EA, Sutcliffe S, Xu J, Grönberg H, Drake CG, et al. Inflammation in prostate carcinogenesis. *Nature Reviews Cancer*. 2007;7(4):256-69.
10. Silva TSVd. The role of macroH2A1 in prostatecarcinogenesis. Braga: University of minho 2015.
11. Lee CH, Akin-Olugbade O, Kirschenbaum A. Overview of Prostate Anatomy, Histology, and Pathology. *Endocrinology and Metabolism Clinics of North America*. 2011;40(3):565-75.
12. Bostwick DG, Cheng L. Precursors of prostate cancer. 2012;60(1):4-27.

13. Vasioukhin V. Hepsin Paradox Reveals Unexpected Complexity of Metastatic Process. *Cell cycle* (Georgetown, Tex). 2004;3:1394-7.
14. Shen MM, Abate-Shen C. Molecular genetics of prostate cancer: new prospects for old challenges. *Genes Dev.* 2010;24(18):1967-2000.
15. Rosen R, Altwein J, Boyle P, Kirby RS, Lukacs B, Meuleman E, et al. Lower Urinary Tract Symptoms and Male Sexual Dysfunction: The Multinational Survey of the Aging Male (MSAM-7). *European Urology.* 2003;44(6):637-49.
16. Nelson AW, Shah N. *Prostate cancer. Surgery* (Oxford). 2019;37(9):500-7.
17. Descotes J-L. Diagnosis of prostate cancer. *Asian Journal of Urology.* 2019;6(2):129-36.
18. Telesca D, Etzioni R, Gulati R. Estimating Lead Time and Overdiagnosis Associated with PSA Screening from Prostate Cancer Incidence Trends. *Biometrics.* 2008;64(1):10-9.
19. Buyyounouski MK, Choyke PL, McKenney JK, Sartor O, Sandler HM, Amin MB, et al. Prostate cancer – major changes in the American Joint Committee on Cancer eighth edition cancer staging manual. *CA: A Cancer Journal for Clinicians.* 2017;67(3):245-53.
20. Saini S. PSA and beyond: alternative prostate cancer biomarkers. *Cell Oncol (Dordr).* 2016;39(2):97-106.
21. Tan MHE, Li J, Xu HE, Melcher K, Yong E-I. Androgen receptor: structure, role in prostate cancer and drug discovery. *Acta Pharmacol Sin.* 2015;36(1):3-23.
22. Bjartell A, Montironi R, Berney DM, Egevad L. Tumour markers in prostate cancer II: Diagnostic and prognostic cellular biomarkers. *Acta Oncologica.* 2011;50(sup1):76-84.
23. Plourde G. Chapter 9 - Case Report #9—Biomarkers of Prostate Cancer. In: Plourde G, editor. *Prostate Cancer: Academic Press; 2018.* p. 93-105.
24. Sartori DA, Chan DW. Biomarkers in prostate cancer: what's new? *Curr Opin Oncol.* 2014;26(3):259-64.
25. Hessels D, Schalken JA. The use of PCA3 in the diagnosis of prostate cancer. *Nature Reviews Urology.* 2009;6(5):255-61.

26. van der Toom EE, Axelrod HD, de la Rosette JJ, de Reijke TM, Pienta KJ, Valkenburg KC. Prostate-specific markers to identify rare prostate cancer cells in liquid biopsies. *Nature Reviews Urology*. 2019;16(1):7-22.
27. Ganguly SS, Li X, Miranti CK. The host microenvironment influences prostate cancer invasion, systemic spread, bone colonization, and osteoblastic metastasis. *Front Oncol*. 2014;4:364-.
28. Jin J-K, Dayyani F, Gallick GE. Steps in prostate cancer progression that lead to bone metastasis. 2011;128(11):2545-61.
29. Fabisiewicz A, Grzybowska E. CTC clusters in cancer progression and metastasis. *Medical Oncology*. 2017;34(12).
30. Shibue T, Weinberg RA. Metastatic colonization: Settlement, adaptation and propagation of tumor cells in a foreign tissue environment. *Seminars in Cancer Biology*. 2011;21(2):99-106.
31. Massagué J, Obenauf AC. Metastatic colonization by circulating tumour cells. *Nature*. 2016;529(7586):298-306.
32. Diamond E, Lee GY, Akhtar N, Kirby B, Giannakakou P, Tagawa S, et al. Isolation and characterization of circulating tumor cells in prostate cancer. 2012;2(131).
33. Ribeiro-Samy S, Oliveira MI, Pereira-Veiga T, Muínelo-Romay L, Carvalho S, Gaspar J, et al. Fast and efficient microfluidic cell filter for isolation of circulating tumor cells from unprocessed whole blood of colorectal cancer patients. *Scientific Reports*. 2019;9(1):8032.
34. Maheswaran S, Haber DA. Circulating tumor cells: a window into cancer biology and metastasis. *Current Opinion in Genetics & Development*. 2010;20(1):96-9.
35. Sun Y, Haglund TA, Rogers AJ, Ghanim AF, Sethu P. Review: Microfluidics technologies for blood-based cancer liquid biopsies. *Analytica Chimica Acta*. 2018;1012:10-29.
36. Lu S-H, Tsai W-S, Chang Y-H, Chou T-Y, Pang S-T, Lin P-H, et al. Identifying cancer origin using circulating tumor cells. *Cancer Biology & Therapy*. 2016;17(4):430-8.

37. Coffelt SB, Hughes R, Lewis CE. Tumor-associated macrophages: Effectors of angiogenesis and tumor progression. *Biochimica et Biophysica Acta (BBA) - Reviews on Cancer*. 2009;1796(1):11-8.
38. Yang L, Zhang Y. Tumor-associated macrophages: from basic research to clinical application. *Journal of Hematology & Oncology*. 2017;10(1):58.
39. Solinas G, Germano G, Mantovani A, Allavena P. Tumor-associated macrophages (TAM) as major players of the cancer-related inflammation. 2009;86(5):1065-73.
40. Chanmee T, Ontong P, Konno K, Itano N. Tumor-associated macrophages as major players in the tumor microenvironment. *Cancers*. 2014;6(3):1670-90.
41. Allavena P, Sica A, Solinas G, Porta C, Mantovani A. The inflammatory micro-environment in tumor progression: the role of tumor-associated macrophages. *Critical reviews in oncology/hematology*. 2008;66(1):1-9.
42. Adams DL, Martin SS, Alpaugh RK, Charpentier M, Tsai S, Bergan RC, et al. Circulating giant macrophages as a potential biomarker of solid tumors. *Proc Natl Acad Sci U S A*. 2014;111(9):3514-9.
43. Hume R, West JT, Malmgren RA, Chu EA. Quantitative Observations of Circulating Megakaryocytes in the Blood of Patients with Cancer. 1964;270(3):111-7.
44. Raker JW, Taft PD, Edmonds EE. Significance of Megakaryocytes in the Search for Tumor Cells in the Peripheral Blood. 1960;263(20):993-6.
45. Mu Z, Wang C, Ye Z, Rossi G, Sun C, Li L, et al. Prognostic values of cancer associated macrophage-like cells (CAML) enumeration in metastatic breast cancer. *Breast Cancer Research and Treatment*. 2017;165(3):733-41.
46. Adams DL, Adams DK, Alpaugh RK, Cristofanilli M, Martin SS, Chumsri S, et al. Circulating Cancer Associated Macrophage-Like Cells Differentiate Malignant Breast Cancer and Benign Breast Conditions. *Cancer Epidemiology Biomarkers & Prevention*. 2016:cebp.1221.2015.
47. Mong J, Tan M-H. Size-Based Enrichment Technologies for Non-cancerous Tumor-Derived Cells in Blood. *Trends in Biotechnology*. 2018;36(5):511-22.

48. Zhang J, Yan S, Yuan D, Alici G, Nguyen N-T, Ebrahimi Warkiani M, et al. Fundamentals and applications of inertial microfluidics: a review. *Lab on a Chip*. 2016;16(1):10-34.
49. Chen J, Li J, Sun Y. Microfluidic approaches for cancer cell detection, characterization, and separation. *Lab on a Chip*. 2012;12(10):1753-67.
50. Chandran KB, Rittgers SE, Yoganathan AP. *Biofluid mechanics: The human circulation*, second edition 2012. 1-420 p.
51. Militký J. 13 - Tensile failure of polyester fibers. In: Bunsell AR, editor. *Handbook of Properties of Textile and Technical Fibres (Second Edition)*: Woodhead Publishing; 2018. p. 421-514.
52. Pinto EMV. *Estudo experimental de escoamentos fisiológicos em microcanais fabricados por xurografia*. Bragança: Escola Superior de Tecnologia e Gestão; 2012.
53. Pinho D. *Blood rheology and red blood cell migration in microchannel flow*. Porto Faculdade de Engenharia da Universidade do Porto; 2018.
54. Qiu Y, Myers DR, Lam WA. The biophysics and mechanics of blood from a materials perspective. *Nature Reviews Materials*. 2019;4(5):294-311.
55. Brust M, Schaefer C, Doerr R, Pan L, Garcia M, Arratia PE, et al. Rheology of Human Blood Plasma: Viscoelastic Versus Newtonian Behavior. *Physical Review Letters*. 2013;110(7):078305.
56. Lima R, Ishikawa T, Imai Y, Yamaguchi T. *Blood flow behavior in microchannels: Past, current and future trends*. *Single and Two-Phase Flows on Chemical and Biomedical Engineering*. 2012.
57. Antfolk M, Laurell T. Continuous flow microfluidic separation and processing of rare cells and bioparticles found in blood – A review. *Analytica Chimica Acta*. 2017;965:9-35.
58. Barrett LM, Simmons BA. Cell Sorting. In: Li D, editor. *Encyclopedia of Microfluidics and Nanofluidics*. Boston, MA: Springer US; 2008. p. 224-34.
59. Iliescu FS, Poenar DP, Yu F, Ni M, Chan KH, Cima I, et al. Recent advances in microfluidic methods in cancer liquid biopsy. *Biomicrofluidics*. 2019;13(4):041503.

60. Adams D, Tang C-M, Makarova O, Zhu P, Li S, Amstutz P, inventors Capture, identification and use of a new biomarker of solid tumors in body fluids. US2015.
61. TANG C-M, ADAMS D, inventors; Creatv Micro Tech , Inc, assignee. USE OF CIRCULATING CELL BIOMARKERS IN THE BLOOD FOR DETECTION AND DIAGNOSIS OF DISEASES AND METHODS OF ISOLATING THEM. US2018.
62. Catarino SO, Rodrigues RO, Pinho D, Miranda JM, Minas G, Lima R. Blood Cells Separation and Sorting Techniques of Passive Microfluidic Devices: From Fabrication to Applications. *Micromachines (Basel)*. 2019;10(9):593.
63. Ajanth P, Sudeepthi A, Sen AK. Microfluidics Technology for Label-Free Isolation of Circulating Tumor Cells. *Journal of The Institution of Engineers (India): Series C*. 2020;101(6):1051-71.
64. Pødenphant M, Ashley N, Koprowska K, Mir KU, Zalkovskij M, Bilenberg B, et al. Separation of cancer cells from white blood cells by pinched flow fractionation. *Lab on a Chip*. 2015;15(24):4598-606.
65. Bodmer W, Podenphant M, Ashley N, Koprowska K, Mir K, Zalkovskij M, et al. Separation of cancer cells from white blood cells by pinched flow fractionation. 2015;15(24):4598-606.
66. Okano H, Konishi T, Suzuki T, Suzuki T, Ariyasu S, Aoki S, et al. Enrichment of circulating tumor cells in tumor-bearing mouse blood by a deterministic lateral displacement microfluidic device. *Biomedical Microdevices*. 2015;17(3):59.
67. Liu Z, Huang F, Du J, Shu W, Feng H, Xu X, et al. Rapid isolation of cancer cells using microfluidic deterministic lateral displacement structure. 2013;7(1):011801.
68. Bhagat AA, Bhagat S, Hou H, Li L, Lim CT, Han J. DEAN FLOW FRACTIONATION (DFF) ISOLATION OF CIRCULATING TUMOR CELLS (CTCs) FROM BLOOD. 2020.
69. Chen Y, Li P, Huang P-H, Xie Y, Mai JD, Wang L, et al. Rare cell isolation and analysis in microfluidics. *Lab on a Chip*. 2014;14(4):626-45.
70. Khoo BL, Warkiani ME, Tan DS-W, Bhagat AAS, Irwin D, Lau DP, et al. Clinical Validation of an Ultra High-Throughput Spiral Microfluidics for the Detection and Enrichment of Viable Circulating Tumor Cells. *PLoS One*. 2014;9(7):e99409.

71. Zhang X, Haswell S. Materials Matter in Microfluidic Devices. *MRS Bulletin*. 2006;31.
72. Fiorini GS, Chiu DT. Disposable microfluidic devices: fabrication, function, and application. *BioTechniques*. 2005;38(3):429-46.
73. Becker H, Locascio LE. Polymer microfluidic devices. *Talanta*. 2002;56(2):267-87.
74. Campo Ad, Greiner C. SU-8: a photoresist for high-aspect-ratio and 3D submicron lithography. *Journal of Micromechanics and Microengineering*. 2007;17(6):R81-R95.
75. Faustino V, Catarino SO, Lima R, Minas G. Biomedical microfluidic devices by using low-cost fabrication techniques: A review. *Journal of Biomechanics*. 2016;49(11):2280-92.
76. Kim P, Kwon KW, Park M, Lee S, Kim SM, Suh K. Soft Lithography for Microfluidics: a Review. *Biochip Journal*. 2008;2(1).
77. Tang S, Whitesides GM. Basic microfluidic and soft lithographic techniques. *Optofluidics: Fundamentals, Devices and Applications*. 2010:7-28.
78. Xiong L, Chen P, Zhou Q. Adhesion promotion between PDMS and glass by oxygen plasma pre-treatment. *Journal of Adhesion Science and Technology*. 2014;28(11):1046-54.
79. Katzenberg F. Plasma-bonding of poly(dimethylsiloxane) to glass. *e-Polymers*. 2005;5.
80. Lopes R, Rodrigues RO, Pinho D, Garcia V, Schütte H, Lima R, et al., editors. Low cost microfluidic device for partial cell separation: Micromilling approach. 2015 IEEE International Conference on Industrial Technology (ICIT); 2015 17-19 March 2015.
81. Ku X, Zhang Z, Liu X, Chen L, Li G. Low-cost rapid prototyping of glass microfluidic devices using a micromilling technique. *Microfluidics and Nanofluidics*. 2018;22(8):82.
82. He Y, Wu Y, Fu J-z, Gao Q, Qiu J-j. Developments of 3D Printing Microfluidics and Applications in Chemistry and Biology: a Review. *Electroanalysis*. 2016;28(8):1658-78.
83. Amin R, Knowlton S, Hart A, Yenilmez B, Ghaderinezhad F, Katebifar S, et al. 3D-printed microfluidic devices. *Biofabrication*. 2016;8(2):022001.

84. Bhagat AAS, Kuntaegowdanahalli SS, Papautsky I. Continuous particle separation in spiral microchannels using dean flows and differential migration. *Lab on a Chip*. 2008;8(11):1906-14.
85. Mitra P, Dutta S, Nagahanumaiah, Hens A. Separation of particles in spiral micro-channel using Dean's flow fractionation. *Journal of the Brazilian Society of Mechanical Sciences and Engineering*. 2020;42(8):405.
86. Warkiani ME, Khoo BL, Wu L, Tay AKP, Bhagat AAS, Han J, et al. Ultra-fast, label-free isolation of circulating tumor cells from blood using spiral microfluidics. *Nature Protocols*. 2016;11(1):134-48.
87. Carvalho S, Abreu CM, Ferreira D, Lima L, Ferreira JA, Santos LL, et al. Phenotypic Analysis of Urothelial Exfoliated Cells in Bladder Cancer via Microfluidic Immunoassays: Sialyl-Tn as a Novel Biomarker in Liquid Biopsies. 2020;10(1774).
88. Musson RA. Human monocyte maturation/differentiation during in vitro culture. *Survey of Immunologic Research*. 1983;2(3):246-51.
89. D'Onofrio C, Paradisi F. In-vitro Differentiation of Human Monocytes into Mature Macrophages during Long-Term Cultures. *Immunobiology*. 1983;164(1):13-22.
90. McNally AK, Anderson JM. Interleukin-4 induces foreign body giant cells from human monocytes/macrophages. Differential lymphokine regulation of macrophage fusion leads to morphological variants of multinucleated giant cells. *Am J Pathol*. 1995;147(5):1487-99.
91. Hudson M, Markowitz A, Gutterman J, Knowles R, Snyder J, Kleinerman E. Effect of recombinant human interleukin 4 on human monocyte activity. *Cancer research*. 1990;50:3154-8.
92. Enelow RI, Sullivan GW, Carper HT, Mandell GL. Induction of multinucleated giant cell formation from in vitro culture of human monocytes with interleukin-3 and interferon-gamma: comparison with other stimulating factors. *American journal of respiratory cell and molecular biology*. 1992;6(1):57-62.

93. Möst J, Spötl L, Mayr G, Gasser A, Sarti A, Dierich MP. Formation of Multinucleated Giant Cells In Vitro Is Dependent on the Stage of Monocyte to Macrophage Maturation. *Blood*. 1997;89(2):662-71.
94. McNally AK, Anderson JM. Macrophage fusion and multinucleated giant cells of inflammation. *Advances in experimental medicine and biology*. 2011;713:97-111.
95. Sutton JS, Weiss L. Transformation of monocytes in tissue culture into macrophages, epithelioid cells, and multinucleated giant cells. An electron microscope study. *J Cell Biol*. 1966;28(2):303-32.
96. Utsunomiya Y, Omura K, Yokoo T, Imasawa T, Kawamura T, Abe A, et al. Macrophage-colony stimulating factor (M-CSF) enhances proteinuria and recruitment of macrophages into the glomerulus in experimental murine nephritis. *Clinical and experimental immunology*. 1996;106(2):286-96.
97. Ushach I, Zlotnik A. Biological role of granulocyte macrophage colony-stimulating factor (GM-CSF) and macrophage colony-stimulating factor (M-CSF) on cells of the myeloid lineage. *J Leukoc Biol*. 2016;100(3):481-9.
98. Khwaja A, Johnson B, Addison IE, Yong K, Ruthven K, Abramson S, et al. In vivo effects of macrophage colony-stimulating factor on human monocyte function. 1991;77(1):25-31.
99. Kuntaegowdanahalli SS, Bhagat AAS, Kumar G, Papautsky I. Inertial microfluidics for continuous particle separation in spiral microchannels. *Lab on a Chip*. 2009;9(20):2973-80.
100. Bhagat AA, Kuntaegowdanahalli S, Papautsky I. Inertial microfluidics for continuous particle filtration and extraction. *Microfluidics and Nanofluidics*. 2008;7:217-26.
101. Seo J, Lean MH, Kole A. Membrane-free microfiltration by asymmetric inertial migration. 2007;91(3):033901.
102. Karimi A, Yazdi S, Ardekani AM. Hydrodynamic mechanisms of cell and particle trapping in microfluidics. *Biomicrofluidics*. 2013;7(2):21501.
103. Nivedita N, Papautsky I. Continuous separation of blood cells in spiral microfluidic devices. 2013;7(5):054101.

104. Choi S, Song S, Choi C, Park J-K. Continuous blood cell separation by hydrophoretic filtration. *Lab on a Chip*. 2007;7(11):1532-8.
105. Bhagat AAS, Hou HW, Li LD, Lim CT, Han J. Pinched flow coupled shear-modulated inertial microfluidics for high-throughput rare blood cell separation. *Lab on a Chip*. 2011;11(11):1870-8.
106. Hou HW, Petchakup C, Tay HM, Tam ZY, Dalan R, Chew DEK, et al. Rapid and label-free microfluidic neutrophil purification and phenotyping in diabetes mellitus. *Scientific Reports*. 2016;6(1):29410.
107. Chiu P-L, Chang C-H, Lin Y-L, Tsou P-H, Li B-R. Rapid and Safe Isolation of Human Peripheral Blood B and T Lymphocytes through Spiral Microfluidic Channels. *Scientific Reports*. 2019;9(1):8145.
108. Warkiani ME, Guan G, Luan KB, Lee WC, Bhagat AAS, Kant Chaudhuri P, et al. Slanted spiral microfluidics for the ultra-fast, label-free isolation of circulating tumor cells. *Lab on a Chip*. 2014;14(1):128-37.
109. Herrmann N, Neubauer P, Birkholz M. Spiral microfluidic devices for cell separation and sorting in bioprocesses. 2019;13(6):061501.
110. Zhou J, Tu C, Liang Y, Huang B, Fang Y, Liang X, et al. Isolation of cells from whole blood using shear-induced diffusion. *Scientific Reports*. 2018;8(1):9411.
111. Hou HW, Warkiani ME, Khoo BL, Li ZR, Soo RA, Tan DS-W, et al. Isolation and retrieval of circulating tumor cells using centrifugal forces. *Scientific Reports*. 2013;3(1):1259.
112. Pamme N. Continuous flow separations in microfluidic devices. *Lab on a Chip*. 2007;7(12):1644-59.
113. Huang X, Gao P, Song Y, Sun J, Chen X, Zhao J, et al. Meta-analysis of the prognostic value of circulating tumor cells detected with the CellSearch System in colorectal cancer. *BMC Cancer*. 2015;15(1):202.
114. Coumans F, Terstappen L. Detection and Characterization of Circulating Tumor Cells by the CellSearch Approach. *Methods in molecular biology (Clifton, NJ)*. 2015;1347:263-78.

115. Guo T., Wang C.S., Wang W., Y. L. Culture of Circulating Tumor Cells - Holy Grail and Big Challenge. *Int J Cancer Clin Res* 2016;3:065.
116. Low WS, Wan Abas WAB. Benchtop Technologies for Circulating Tumor Cells Separation Based on Biophysical Properties. *BioMed Research International*. 2015;2015:239362.
117. Adams DL, Adams DK, Alpaugh RK, Cristofanilli M, Martin SS, Chumsri S, et al. Circulating Cancer-Associated Macrophage-Like Cells Differentiate Malignant Breast Cancer and Benign Breast Conditions. *Cancer Epidemiol Biomarkers Prev*. 2016;25(7):1037-42.
118. Mu Z, Wang C, Ye Z, Rossi G, Sun C, Li L, et al. Prognostic values of cancer associated macrophage-like cells (CAML) enumeration in metastatic breast cancer. *Breast cancer research and treatment*. 2017;165(3):733-41.
119. Andree KC, van Dalum G, Terstappen LWMM. Challenges in circulating tumor cell detection by the CellSearch system. *Mol Oncol*. 2016;10(3):395-407.
120. Kim TH, Yoon HJ, Stella P, Nagrath S. Cascaded spiral microfluidic device for deterministic and high purity continuous separation of circulating tumor cells. 2014;8(6):064117.
121. Lee WC, Bhagat AAS, Huang S, Van Vliet KJ, Han J, Lim CT. High-throughput cell cycle synchronization using inertial forces in spiral microchannels. *Lab on a Chip*. 2011;11(7):1359-67.

ANNEXES

Authors: Ana Rita Cacho, Dra. Sandra Carvalho, Dra. Diana Pinho, Prof. Paulo Freitas, Prof. Rui Lima, Dra. Marta Oliveira.

Article title: Opening Doors for CAMLs in liquid biopsies.

Journal title: to be defined.

Year: in preparation.